

Efficient Polymeric Solutions for Oil Spill Remediation

by

Fereshte Damavandi

A thesis submitted in partial fulfillment of the requirements for the degree of

Doctor of Philosophy

in

Chemical Engineering

Department of Chemical and Materials Engineering

University of Alberta

© Fereshte Damavandi, 2022

Abstract

Oil spills are a worldwide concern that threaten the environment, ecosystems, human health, and economy. Conventional methods to combat oil spills, such as in-situ burning, booms and skimmers, dispersants, and biodegradation are not effective enough. A more efficient technology is needed to contain future oil spill incidents. For example, the lack of efficient oil spill responses in the BP (British Petroleum) spill in the Gulf of Mexico caused massive, short- and long-term environmental and industrial damages that could have been minimized with better methods were available at the time.

Oil solidifiers, a new class of clean-up technology, have been recently introduced for practical and efficient remediation of oil spills. In this thesis, I developed two different types of oil spill solidifiers: a magnetic polymer nanocomposite and a polymer organogelator. I investigated the oil removal of these two solidifiers by removing high and low viscosity oil from the water surface. I also evaluated the effectiveness of the solidification performance of the polymer organogelator to find the most efficient operational conditions.

The main findings of this thesis were reported in three studies:

1. Development of magnetic polystyrene nanocomposite by grafting polystyrene chains on the surface of silica-coated iron oxide nanoparticles (IONP) and use as an oil solidifier. Styrene was polymerized on the surface of iron oxide nanoparticles using surface-initiated atom transfer radical polymerization (SI-ATRP) to make polystyrene-grafted silica-coated IONP (PS-SiO₂-IONP). The chemical and physical properties of PS-SiO₂-IONP were measured by field emission high-resolution scanning electron microscopy (SEM), X-ray diffraction (XRD), Fourier-transform infrared (FTIR) spectroscopy, and X-ray photoelectron spectroscopy (XPS). Polystyrene provided the required porous structure,

hydrophobicity, and oleophilicity for excellent oil absorption. The results showed that the oil absorption capacity of the polystyrene magnetic nanocomposite was 5 g oil/g absorbent for diluted bitumen and 3 g oil/g absorbent for diesel. I also made polystyrene with different molecular weights and blended them with PS-SiO₂-IONP. Interestingly, the oil absorption tests showed that a blend with a weight composition of 91 % polystyrene and 9 % PS-SiO₂-IONP nanocomposite had an oil absorption capacity equal to the pure PS-SiO₂-IONP nanocomposite.

2. Synthesis of a novel phase-selective poly(styrene-*co*-10-undecenoic acid) (PS10UA) organogelator and use as an oil solidifier for oil recovery from biphasic oil/water mixtures. The novel copolymers performed well, gelling diluted bitumen and diesel spilled on water. The oil gelling ability of PS10UA depends on the 10-undecenoic acid (10UA) content and oil type. PS10UA with 10UA molar composition of 4.5 % and 3.5 % had the highest oil removal efficiency for diluted bitumen and diesel, respectively. Rheological measurements confirmed the mechanical strength and SEM revealed the fibrillar morphology and 3D network structure of the gels. FTIR measurements of the gels suggested that hydrogen bonding is mainly responsible for the gel formation, while Van der Waals forces and π - π stacking interactions promote the gelation.
3. Investigation of solidifier:oil ratio and contact time of PS10UA on solidification effectiveness in removing diluted bitumen from the water surface. PS10UA was most efficient at a solidifier:oil ratio of 1:8 after 15 minutes. I also studied the influence of the bulk density (particle size) of PS10UA on its oil removal performance and found that PS10UA organogelators with lower bulk density performed better by speeding up the dissolution process.

Preface

Chapter 2 has been partially published in Fereshte Damavandi, João B.P. Soares, Polystyrene magnetic nanocomposite blend: An effective, facile, and economical alternative in oil spill removal applications, *Chemosphere* **2022** 286, Part 2. I designed the experiments, made the polymers, analyzed the data, wrote the first draft and revised the manuscript.

Chapter 3 has been accepted for publication, Fereshte Damavandi, João B.P. Soares, Facile and efficient phase-selective powder polymer organogelator for oil spill remediation, *Langmuir* **2022**. I designed the experiments, synthesized the polymers, analyzed the data, and wrote the first draft and revised the manuscript.

Chapter 4 has been submitted for publication as Fereshte Damavandi, João B.P. Soares, Evaluating the effectiveness of a new polymer organogelator for the solidification of oil spilled on water, *Langmuir* **2022**. I designed the experiments, produced the polymers, analyzed the data, and wrote the first draft and revised the manuscript.

In all the papers, J. Soares supervised the research and contributed to the manuscript composition and edits.

Acknowledgement

My deepest gratitude goes to my advisor, Prof. João Soares, without whose guidance, encouragement, and support this work would not have been completed. He not only taught me “how to science” and gave me insightful advice on my research, but also showed me what a great mentor looks like. He has been always patient and supportive. His broad knowledge, experience, encouragement, mentorship, and constructive advice have been of great value for me. He has been always available when I needed his advice, and it has been my great honor to work under his supervision and to learn how to develop my personality.

I also would like to thank my peers and colleagues who have helped me in accomplishing this thesis. My thanks go to Dr. Saied Mehdiabadi for his help and constructive scientific discussions, Dr. Fernanda Lopes Motta for her help and support, and Dr. Bruno T. Luppi for his help for sample analysis.

My gratitude also goes to all my friends for the support they offered me whilst pursuing this research.

I am forever indebted to my parents, Maryam and Mosayeb for their support and encouragement throughout my life. I also would like to express my gratitude to my siblings, Ali Akbar, Akram, Bakhtyar, Pourdad, Nourjahan, and Pari. I immensely thank them for their inspiration and endless support. Finally, and most importantly, I reserve the rest of my acknowledgements for my beloved husband Ali, whose love, friendship, and support have been real blessing. I would not have been able to go through this without his support.

Fereshte Damavandi

Table of Contents

Chapter 1: Introduction	1
1.1 Background	1
1.1.1 Motivation.....	1
1.2 Literature Review.....	2
1.2.1 Technologies for Oil Spill Control	2
1.2.1.1 Physical Methods	2
1.2.1.1.1 Sorbents.....	3
1.2.1.2 In-Situ Burning	5
1.2.1.3 Bioremediation Methods.....	5
1.2.1.4 Chemical Methods	5
1.2.1.4.1 Chemical Dispersants.....	5
1.2.1.4.2 Solidifiers.....	6
1.2.1.4.3 Gelators	7
1.2.1.4.4 Low Molecular Weight Organogelators	9
1.2.1.4.5 Polymer Organogelators	10
1.2.1.5 Effectiveness of Solidifiers	12
1.3 Thesis Objectives	12
1.4 Thesis Outline	13
Chapter 2: Polystyrene Magnetic Nanocomposite Blend: An Effective, Facile, and Economical Alternative in Oil Spill Removal Applications.....	15

2.1 Introduction.....	15
2.2 Material and Methods	18
2.2.1 Materials	18
2.2.2 Synthesis of Superparamagnetic Iron Oxide Nanoparticles, IONPs	19
2.2.3 Synthesis of SiO ₂ -IONP.....	19
2.2.4 Functionalization of SiO ₂ -IONP with an ATRP Initiator (Br-SiO ₂ -IONP).....	20
2.2.5 Reverse ATRP of Styrene	20
2.2.6 Synthesis of Polystyrene Grafts on Br-SiO ₂ -IONP (PS-SiO ₂ -IONP).....	21
2.2.7 Nanocomposite Characterization	21
2.2.8 Oil Absorption Experiments	22
2.3 Result and Discussion	23
2.3.1 Synthesis and Characterization of PS-SiO ₂ -IONP.....	23
2.3.2 Synthesis of Polystyrene by Reverse ATRP	26
2.3.3 Synthesis of Polystyrene Grafts on Br-SiO ₂ -IONP by SI-ATRP	29
2.3.4 Oil Absorption Performance	31
2.4 Conclusion	35
Chapter 3: Efficient Phase-Selective Powder Polymer Organogelator for Oil Spill Remediation	36
3.1 Introduction.....	36
3.2 Materials and Methods.....	40
3.2.1 Materials	40
3.2.2 Characterization Techniques.....	40
3.2.3 Copolymer Synthesis	41

3.2.4 Minimum Gelation Concentration	42
3.2.5 Oil Spill Removal Using Polymer Organogelators.....	42
3.2.6 Determination of Gel-to-Sol Transition Temperature (T _{g-s})	43
3.3 Result and Discussion.....	43
3.3.1 Copolymer Synthesis	43
3.3.2 Measuring the Minimum Gelation Concentration	44
3.3.3 Room-Temperature Phase-Selective Gelation.....	45
3.3.4 Gelation Mechanism	48
3.4 Conclusions.....	52
Chapter 4: Evaluating the Effectiveness of a New Polymer Organogelator for the Solidification of Oil Spill on Water	53
4.1 Introduction.....	53
4.2 Materials and Methods.....	55
4.3 Experimental Procedure.....	56
4.4 Result and Discussion.....	56
4.4.1 Effect of Solid-to-Oil Ratio (SOR).....	56
4.4.2 Effect of Oil and Solidifier Contact Time.....	57
4.4.3 Effect of Solidifier Powder Size and Bulk Density	59
4.5 Conclusion	62
Chapter 5: Conclusions and Recommendations	63
5.1 Conclusions.....	63
5.2 Recommendations.....	65

References.....	67
Appendix A: Supplementary Information for Chapter 2	86
Appendix B: Supplementary Information for Chapter 3	91
Appendix C: Supplementary Information for Chapter 4	95

List of Tables

Table 2.1 Polymerization conditions and polystyrene properties.	21
Table 3.1 Poly(styrene- <i>co</i> -10-undecenoic acid) with different copolymer compositions.	41
Table 3.2 Density and viscosity of diluted bitumen and diesel at 23 °C.	42
Table 3.3 Gelation properties of PS10UA in dilbit and diesel at room temperature	45
Table 4.1 Particle sizes (p.s.) and bulk densities of POS samples.	59
Table A.1 PS/PS-SiO ₂ -IONP blends used in oil removal.	90

List of Figures

Figure 1.1. Summary of typical annual oil spills in Canada.[1]	2
Figure 1.2. Conventional oil spill remediation methods [4]	3
Figure 1.3. Nanomaterials-based technologies for oil spill recovery. [13].....	4
Figure 1.4. In-situ burning methodology to remove oil spill from the water surface.[1]	5
Figure 1.5. Solidifiers and their subclasses intended for application in oil spill	6
Figure 1.6. Schematic representation of oil sorption into the polymer matrix, turning to a semi-solid mass. [25]	7
Figure 1.7. Schematic representation of gelation; a) gelation via H-bonding, b) gelation via π -Staking, c) H-bonded induced fibril, d) π - Staking induced fibril, e) intermolecular bonded fibre, f) 3D gel network. [4]	8
Figure 1.8. Schematic representation of oil spill containment using LMWO. [4].....	9
Figure 1.9. schematic representation of three-dimensional network using polymer gelators. [26]	10
Figure 2.1. Synthesis of PS-SiO ₂ -IONP nanocomposite.	18
Figure 2.2. Micrographs of: a) IONP (SEM), b) SiO ₂ -IONP (SEM), c) PS-SiO ₂ -IONP (SEM), and d) SiO ₂ -IONP (TEM).	24
Figure 2.3. XPS spectra: a) IONP, b) SiO ₂ -IONP, c) Br-SiO ₂ -IONP, d) high-resolution XPS of carbon regions of Br-SiO ₂ -IONP, e) XPS spectra of PS-SiO ₂ -IONP, and f) high resolution XPS of carbon regions of PS-SiO ₂ -IONP.....	28
Figure 2.4. a) Dependence of number average molecular weight, Mn, on monomer conversion, b) polymerization kinetics plot for the reverse ATRP of styrene.	29

Figure 2.5. a) Photographs of diluted bitumen removal from the water surface with PS-SiO ₂ -IONP under a magnetic field and, b) oil absorption capacity of PS-SiO ₂ -IONP at different times for diesel and diluted bitumen.....	32
Figure 2.6. a) Photograph images of removal of diluted bitumen from the water surface by PS/PS-SiO ₂ -IONP blends under a magnetic field and b) oil absorption capacity of PS/PS-SiO ₂ -IONP blends for diesel and diluted bitumen after 5 min.....	34
Figure 3.1. A) ¹ H-NMR of sample PS10UA-4, B) Structure of PS10UA, C) FTIR spectrum of sample PS10UA-4.....	44
Figure 3.2 a) Dilbit layer on water, b) Dissolution of PS10UA powder in dilbit, c) Gel removal with a spatula.	46
Figure 3.3 Dynamic rheology studies of: a) PS10UA-3 in dilbit, b) PS10UA-4 in dilbit, c) PS10UA-3 in diesel, d) PS10UA-4 in diesel. All experiments were done at a constant strain of 1 % and 15 mg polymer/100 μL oil.....	47
Figure 3.4. SEM images of dried dilbit gel formed with: a) PS10UA-3, top view, b) PS10UA-3, top view, c) PS10UA-4, edge, d) PS10UA-4, top view. All samples were formed using a ratio of 15% (w/v) organogelator to dilbit.....	48
Figure 3.5. FTIR spectra of: a) PS10UA-3 powder, b) PS10UA-3/diesel gel, and c) PS10UA-4/diesel gel.	49
Figure 3.6. Tentative gelation mechanism of PS10UA.	51
Figure 4.1. Dilbit solidification with poly(styrene- <i>co</i> -10-undecenoic acid) at different solidifier-to-oil ratios: a) 1:32 and 1:16, b) 1:8, 1:4, 1:2, and 1:1, c) 1:8, 1:4, 1:2, and 1:1, solidified oil collected with a spatula. Contact time = 30 min.....	57

Figure 4.2. Effect of solidifier and oil contact time: a) 5 min, b) 15 and 30 min, c) 60 and 120 min (because some of the oil adhered to the walls of the petri dish, we repeated the 60 and 120 min tests in a 1000 ml Pyrex dish). SOR = 1:8.....	59
Figure 4.3. POS samples with different particle sizes (p.s.) after passing through the mechanical shaker machine.....	60
Figure 4.4. a) Oil removal experiments of Dilbit using POS with different particle size, SOR = 1:8, 15 min; b) Final solid oil collected using a spatula, SOR of 1:8, 15 min.	62
Figure A. 1. Hydrodynamic size distribution of IONP determined by dynamic light scattering.	86
Figure A. 2. Room temperature hysteresis of IONP (red) and SiO ₂ -IONP (black): a) full hysteresis loop, b) hysteresis in low filed.....	86
Figure A. 3. XRD spectra: a) IONP, b) SiO ₂ -IONP, c) Br-SiO ₂ -IONP, and d) PS-SiO ₂ -IONP...	87
Figure A. 4. FTIR spectra: a) IONP, b) SiO ₂ -IONP, c) Br-SiO ₂ -IONP, and d) PS-SiO ₂ -IONP. .	87
Figure A. 5. TGA thermographs: a) SiO ₂ -IONP, b) Br-SiO ₂ -IONP, and c) PS-SiO ₂ -IONP.....	88
Figure B. 1. HNMR sample spectra of poly(styrene- <i>co</i> -10-undecenoic acid)	92
Figure B. 2. Photographs of vial approach to measure the MGC.	92
Figure B. 3. Structures of poly(styrene- <i>co</i> -methyl-10-undecenoate) and poly(styrene- <i>co</i> -10-undecenoic acid).	93
Figure B. 4. Dynamic rheology studies of absorbed diesel by PSM10UA (15 mg polymer/100 μL oil).....	94
Figure B. 5. Photograph of a) gelled diesel by PS10UA-4 (15 mg polymer/100 μL oil), b) absorbed diesel by PSM10UA (15 mg polymer/100 μL oil)	94
Figure C. 1. Grinder used for milling POS	95

Figure C. 2. Mechanical sieve shaker machine with different sieve mesh sizes (45, 250, 500, 850, 1000 μ). 96

Figure C. 3. Final mat-like gelled-oil at the end of the oil removal experiments of diluted bitumen using POS. SOR of 1:8, 3 h. 97

Nomenclature

10UA	10-undecenoic acid
^1H NMR	proton nuclear magnetic resonance
AIBN	azobisisobutyronitrile
ATR-FTIR	attenuated total reflectance-Fourier-transform infrared
Br-SiO ₂ -IONP	ATRP initiator-functionalized SiO ₂ -IONP
DCE	1,2-dichloroethane
dilbit	diluted bitumen
DLS	dynamic light scattering
dNbpy	4,4'-Dinonyl-2, 2'-dipyridyl
ECCCs	environment and climate change Canada
EG	ethylene glycol
FeCl ₃	Iron chloride
FTIR	Fourier-transform infrared
GPC	gel permeation chromatography
IONP	iron oxide nanoparticles
IR	infrared
LMWOs	low molecular weight organogelators
MWD	molecular weight distribution
NaAc	sodium acetate
OPV	oligo(<i>p</i> -phenylenevinylene)

POS	polymer organogelator solidifier
PS	polystyrene
PS10UA	poly(styrene- <i>co</i> -10-undecenoic acid)
PSOGs	phase-selective organogelators
PS-SiO ₂ -IONP	polystyrene-grafted silica-coated IONP
PS/PS-SiO ₂ -IONP	polystyrene and polystyrene-grafted silica-coated IONP blend
RAFT	reversible addition-fragmentation chain transfer
SEM	scanning electron microscopy
SI-ATRP	surface-initiated atom transfer radical polymerization
SiO ₂ -IONP	silica-coated superparamagnetic iron oxide nanoparticles
SOR	solidifier-to-oil ratio
TEM	Transmission Electron Microscopy
TEOS	tetraethyl orthosilicate
TGA	thermogravimetric analysis
THF	tetrahydrofuran
T _{g-s}	gel-to-sol transition temperature
UPyEMA	2-(((6-(6-methyl- 4[1H]pyrimidionylureido)hexyl)carbamoyl)oxy)ethyl methacrylate
XPS	X-ray photoelectron spectra
XRD	X-ray diffraction

Chapter 1: Introduction

1.1 Background

1.1.1 Motivation

Even though renewable energy sources are growing, most industries still use oil as fuel. On average, 10 to 15 transfers between different modes of transportation are needed between the oil field and the consumer. Oil spills may happen at any time during this transfer.

Our lives depend on oil and petroleum products. For instance, about 260,000 tons of oil and petroleum products are used daily in Canada. Every day, Canada imports about 130,000 tons and exports 220,000 tons – mainly to the United States – of crude oil and other petroleum products.[1]

Figure 1.1 shows the annual number and volume of oil spills in Canada. The frequency of oil spills and the consequent damages they cause the ecosystem encourages the industry and academia to develop technologies for oil spill remediation that can protect human health and avoid, or at least minimize, the negative impact in the environment.

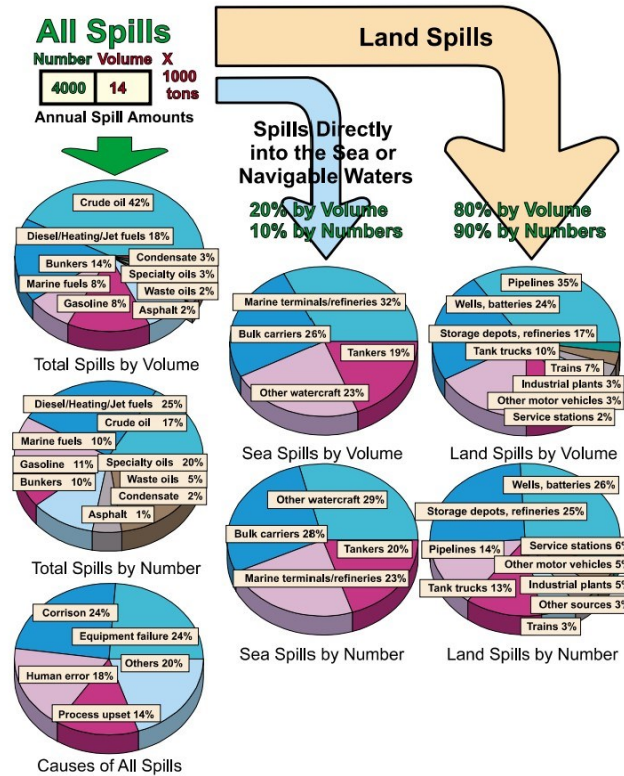


Figure 1.1 Typical annual oil spills in Canada.[1]

1.2 Literature Review

1.2.1 Technologies for Oil Spill Control

Oil spill remediation methods may be classified in four types: physical, chemical, burning, and bioremediation. Sometimes these methods are combined to clean up oil spills more efficiently. Conventional oil spill remediation methods are shown in Figure 1.2.

1.2.1.1 Physical Methods

Although physical methods such as booms [2] and skimmers [3] have been used for years to contain oil spills, they are costly and have low efficiency for spills in turbulent seas, low viscosity oil spills, and oil-in-water emulsion spills. [4] These methods also leave a thin layer of oil after

oil recovery, making the treatment of the residual oil even harder. These drawbacks limit their field applications.

Contrarily, sorbents (adsorbents and absorbents) are economical and efficient physical methods that transform oil spills into semi-solid masses that can be more easily removed from the environment. [5]

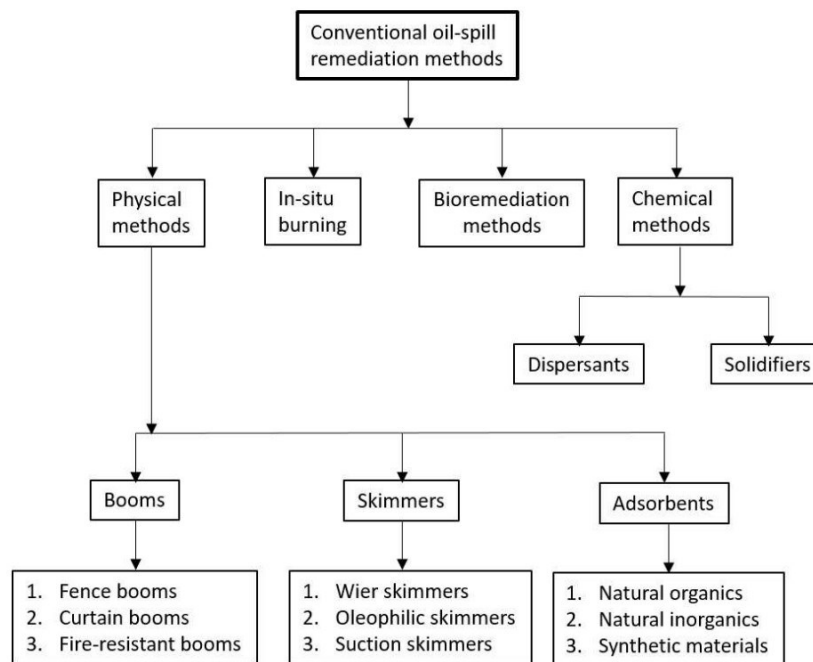


Figure 1.2 Conventional oil spill remediation methods. [4]

1.2.1.1.1 Sorbents

Sorbents are natural or synthetic materials. They bind oil through absorption or adsorption or a combination of both mechanisms. Intermolecular forces, such as van der Waals, π -electron interactions, and hydrophobic effects cause the oil to absorb on network structure or on the surface of the sorbent.[6] Sorbents are the most common materials used to remediate oil spills. [7]–[10] After the Exxon Valdez incident in Prince William Sound in 1989, polymer sorbents have attracted

much attention.[11] A suitable polymer sorbent should combine hydrophobic and oleophilic properties, be inexpensive, and absorb large volumes of oil.[10] Unfortunately, polymer sorbents such as polypropylene sorbents pads still suffer from low oil sorption capacity, are expensive to make and to remove from the environment, require long operation time, and cause secondary pollution.[8]

New approaches, such as nanotechnology, which combine surface chemical composition and nanostructured surfaces, have been proposed as novel strategies to improve sorbent efficiency and reduce the cost of oil spill clean-up operations.[12] Figure 1.3 specifies the current nanomaterial-based oil spill recovery techniques.

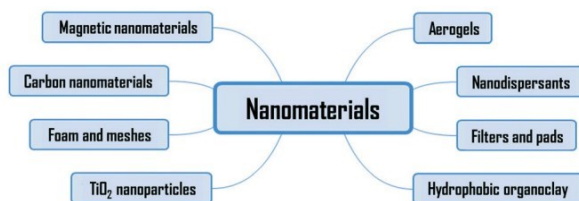


Figure 1.3 Nanomaterials-based technologies for oil spill recovery. [13]

Functionalized magnetic nanoparticles can be prepared by coating polymers onto magnetic cores and used as intelligent polymer sorbents that can be removed from the environment using a magnetic field. Nicolaides et al. introduced this technique in 1998, calling it *CleanMag*. They claimed that their nanocomposite-based oil recovery method could recover 100 % of the spilt oil at cost 30 % lower than other available methods.[13] Many interesting papers have been published in this field, showing that magnetic nanocomposites have the potential to clean up oil spills fastly and efficiently. [14]–[17]

1.2.1.2 In-Situ Burning

In-situ burning is the controlled burning of thick oil layers at or near the spill site.[1] Figure 1.4 shows an in-situ trial burning in Newfoundland. This method has been used in actual oil spills and is acceptable in some countries. Although this method can remove large amounts of oil quickly, it also emits toxic gas and particulate matter into the air and water, threatening the ecosystem.



Figure 1.4 In-situ burning methodology to remove an oil spill from the water surface.[1]

1.2.1.3 Bioremediation Methods

During bioremediation, decomposers, green plants, or their enzymes break down the oil spill. This technique has been used ex- and in-situ for years to remediate oil spills. This environment-friendly technique can be used on all types of shorelines, but it is very slow and works only with light to medium oils.[16]

1.2.1.4 Chemical Methods

1.2.1.4.1 Chemical Dispersants

Chemical dispersant spread the oil on the water surface by reducing its interfacial tension.[18] Chemical dispersants are harmful and may dissolve in water, causing secondary pollution that threatens marine life. The United States Coast Guard reported that 42 million gallons of dispersants were used in 2010 during the British Petroleum oil spill in the Gulf of Mexico. Although this was

the fastest way to remove the massive oil spill, it also had a large impact on the ecosystem that lasted for several years.

1.2.1.4.2 Solidifiers

Solidifiers interact with oil and change its physical state to a cohesive solidified mass, regardless of the mechanism of action. Although the classification of solidifiers may vary from one author to another, all solidifiers must contain the oil spill by turning it into an inert semi-solid mass that can be removed from the water surface. Figure 1.5 shows the classifications of solidifiers suggested by Motta et al.[18]

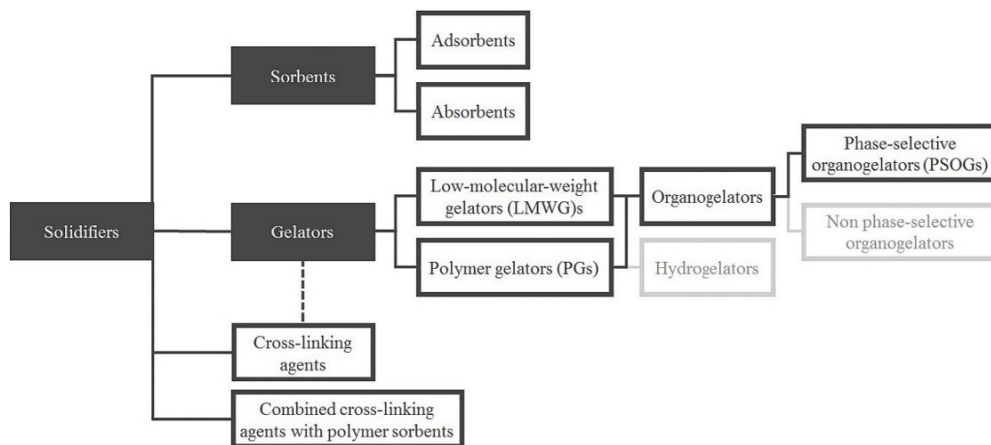


Figure 1.5 Solidifier classification. [18]

Solidifiers have many advantages over other oil spill control methods. First, solidifiers are the only weatherproof countermeasure for oil spills, so they are easier to use in offshore and onshore contaminated areas. Second, solidifiers stop the spread of oil spills immediately. Third, the solidified oil can be scooped out or burned, depending on the location of the oil spill.[19]–[21]

Polymer sorbents and gelators are the two main subclasses of solidifiers.[4], [22] They do not form chemical bonds with oil molecules; instead, intermolecular forces are responsible for turning oil from liquid to semi-solid/solid.[23] Figure 1.6 illustrates oil is absorbed into the polymer matrix.

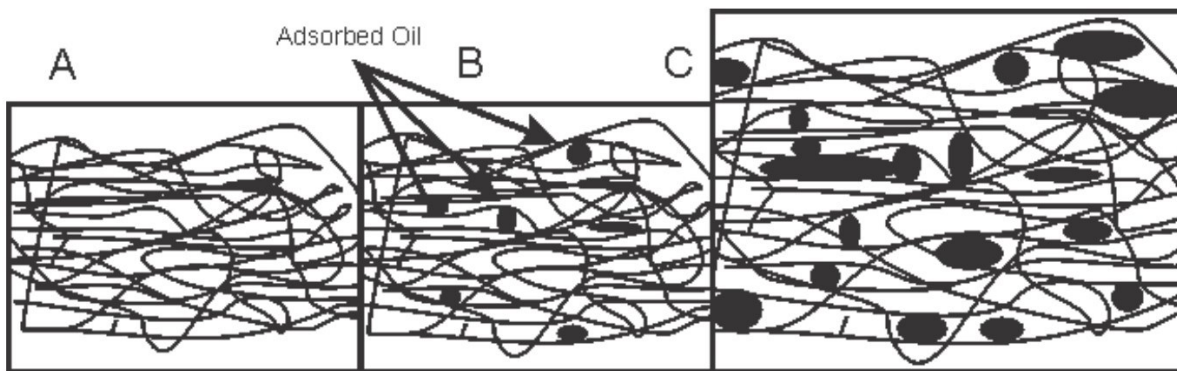


Figure 1.6 Schematic representation of oil sorption into the polymer matrix, turning to a semi-solid mass. [22]

The two other subclasses of solidifiers, cross-linking agents and combined cross-linking agents with polymer sorbents, promote chemical bonding during oil solidification. Cross-linking agents are chemical products that form chemical bonds between hydrocarbons to solidify the oil. Mixing and dissolution are the main limitations of cross-linking agents: they cannot fully penetrate into thick oil layers, leaving the bottom layers unreacted. The final product after cross-linking is a mat-like oil substrate that can be removed from the water surface.

1.2.1.4.3 Gelators

Gelators or organogelators are a subcategory of solidifiers that gel oil. Gelator molecules are generally amphiphilic molecules, having polar and non-polar segments. Gelators must have balanced hydrophobicity and hydrophilicity to facilitate their dissolution in oil while they build the gel network. Figure 1.7 summarizes the intermolecular forces for gel formation: hydrogen bonding, van Der Waal's interactions, and π - π -stacking. [24]–[26] Most organogelators form gel through intermolecular hydrogen bonding and self-assemble into fibrillar structures. [27] The fibrils grow via weak intermolecular forces and then entangle with each other, forming a 3D gel

network that entraps the oil molecules. Similarly, the gelator molecules contain aromatic rings that are rich in π -electron and can self-assemble via π - π stacking to form π -stacked fibrils. [28], [29].

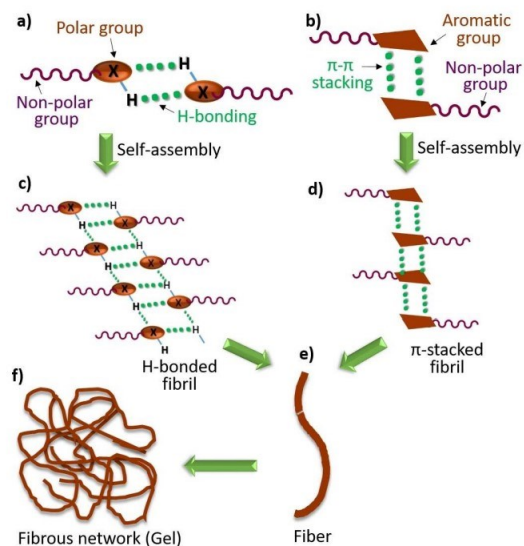


Figure 1.7 Schematic representation of gelation; a) gelation via H-bonding, b) gelation via π - Staking, c) H-bonded induced fibril, d) π - Staking induced fibril, e) intermolecular bonded fibre, f) 3D gel network.

[4]

Low molecular weight organogelators (LMWOs) and polymer organogelators are the two main categories of organogelators.[30], [31] Figure 1.8 shows the application of gelators in oil spill recovery.



Figure 1.8 Schematic representation of oil spill containment using LMWO. [4]

1.2.1.4.4 Low Molecular Weight Organogelators

Low molecular weight organogelators (LMWOs) gel organic solvents and fuels following three main steps:

1. LMWOs dissolve or are suspended in a solvent.
2. The LMWO solubility is decreased using a trigger, such as temperature changes, causing its molecules to self-assemble into long fibres via intermolecular forces. Self-assembling minimizes the interactions between solvents and solute.
3. The fibres interact further by cross-linking to form 3D networks.[32]

Although LMWOs have been known for a while, their application as phase-selective organogelators (PSOGs) has been only investigated for last two decades. The first application of LMWOs as phase selective organogelators for oil spills was reported by Bhattacharya et al.[33] They used an amino acid derivative, *N*-Lauroyl-L-alanine, to gelate oil from oil/water mixtures. The authors first dissolved the gelator by heating the mixture and then cooled it to form the gel. SEM and IR analyses confirmed the formation of a fibrous network via hydrogen bonding. Despite

forming the gel, the heating/cooling cycle limits the application of organogelators in actual oil spill incidents. [34]–[36]

Powder LMWOs have been developed to overcome this limitation. [28], [37]–[40] Recently, Navendu et al. [39] studied a powder gelator-starch blend for the solidification of crude oil at room temperature. The powder gelators, [1-(phenoxy)- β -D-arabinopyranoside, 1-(2-methoxy-phenoxy)- β -D-arabinopyranoside and 1-(3-methoxyphenoxy)- β -D-arabinopyranoside], were prepared and mixed with starch to gel crude oil at room temperature. Although they performed well, their high cost and lengthy preparation procedure limits their application in field operations.

1.2.1.4.5 Polymer Organogelators

Cross-linking sites in the polymer backbones are needed to make physical gels using polymer gelators. Cross-linking sites are formed by conformational changes in the polymer backbone or by the addition of cross-linking groups.[23] Figure 1.9 shows how gels are formed in polymer organogelators.

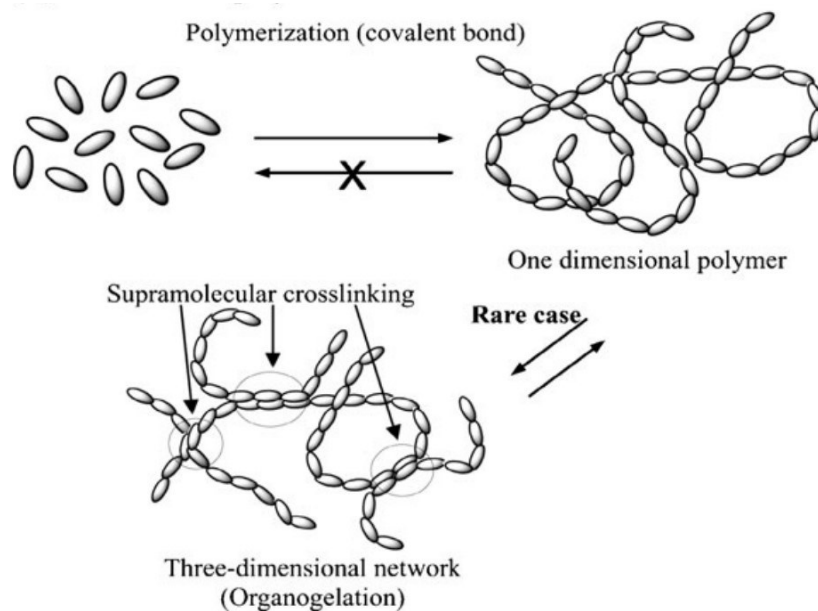


Figure 1.9 Schematic representation of three-dimensional network using polymer gelators. [23]

Since polymer organogelators have some advantages over LMWOs, they recently attracted the attention of researchers looking for solutions in oil spill remediation. Unlike the gels formed with LMWOs, which are prone to collapse after a certain time, the gels formed with polymer organogelators are stable.[31] Better still, making polymer organogelators is simple and inexpensive, making it easy to scale them up field applications.

Polystyrene is a versatile polymer that can form physical gels in organic solvents. Gel formation was reported by Girolamo et al. using isotactic polystyrene in decalin, [41] by Kobayashi et al. using syndiotactic polystyrene in chloroform, carbon tetrachloride and benzene, [42] and by Daniel et al. using syndiotactic polystyrene in binary mixture of 1,2-dichloroethane (DCE) and 1-chlorotetradecane, [43]. Besides being able to form gels in a variety of organic solvents through conformational cross-linking, adding cross-linking groups to the polystyrene backbones increases its gel-formation ability. Ihara et al. reported a polymer organogelator composed of poly(methyl acrylate-co-styrene) with double chain alkylated L-glutamate that formed gel in benzene and cyclohexane/EtOH. [44]

A few investigations have focused on the use of polymer organogelators for oil spill containment. [4]. Nandi et al. recently reported amino acid-based hyperbranched polymers to gel crude oil from oil/water mixtures.[37] They used THF as a carrier solvent to introduce the gelator into the mixture of diesel and water and then removed the gelled diesel.

Phase selectivity, high oil gelation efficiency, low-cost, and environmental friendliness are essential factors for oil solidifies, including polymer organogelators. Fortunately, polymer organogelators can fulfil these requirements due to well-developed techniques to design and synthesise new polymers.

1.2.1.5 Effectiveness of Solidifiers

According to Environment and Climate Change Canada (ECCCs), the effectiveness of a solidifier must be reported as a percentage and is equivalent to the solidifier-to-oil ratio (SOR), where the solidifier with lower SOR has higher efficiency. The performance of a solidifier depends on many variables, including oil composition and amount, weather conditions, air and sea temperature, and surrounding environment. The effectiveness of a solidifier is also related to properties of the solidifier such as hydrophobicity/oleophilicity, surface area, porosity, and bulk density. [45] Although different laboratory effectiveness tests have been developed to evaluate the performance of solidifiers, a standard effectiveness testing protocol has not been developed yet.[22], [46]

1.3 Thesis Objectives

The goal of this thesis was to develop efficient polymeric oil solidifiers to recover high/low viscosity oil from biphasic oil/water mixtures for oil spill applications. This main goal was subdivided into the following projects:

- Develop a magnetic nanocomposite to clean oil spills and test its efficiency with different oils. The advantage of this nanocomposite is that an external magnetic field can be used to collect the oil from the water surface. Its main disadvantages are relatively complex and costly synthesis procedure.
- Find a polymeric alternative to replace with the magnetic nanocomposite to decrease the preparation cost and time.
- Develop a polymeric organogelator that could solidify the oil and change its physical state from a liquid to a semi-solid mass.

- Finally, evaluate the effectiveness of the prepared polymeric solidifier by studying the solidifier-to-oil mass ratio (SOR), oil/solidifier contact time, and the solidifier particle size (bulk density).

1.4 Thesis Outline

This thesis consists of 5 chapters.

Chapter 1 reviews the current oil spill response methods, the challenges associated with them, and the motivation behind this work.

Chapter 2 introduces polystyrene-grafted silica-coated iron oxide nanocomposite (PS-SiO₂-IONP) and its application in oil absorption. In this chapter, we investigated the performance of PS-SiO₂-IONP to recover diluted bitumen and diesel from the water surface. We also investigated the oil absorption capacity of the blend of polystyrene (PS) and PS-SiO₂-IONP. The results obtained in this work are published in Fereshte Damavandi, João B.P. Soares, *An effective, facile, and economical alternative in oil spill removal applications, Chemosphere, Volume 286, Part 2, 2022.*

Chapter 3 introduces poly(styrene-co-10-undecenoic acid)—PS10UA—organogelator to solidify oil from biphasic oil/water mixture. The synthesis of PS10UA, its oil gelation performance, and the gelation mechanism are also discussed in this chapter. The results in this chapter are published in Fereshte Damavandi, João B.P. Soares, *Facile and efficient phase-selective powder polymer organogelator for oil spill remediation, Langmuir, 2022.*

Chapter 4 investigates the effectiveness of the PS10UA organogelator in removing diluted bitumen from the biphasic oil/water mixture. The influence of the operational parameters and physical properties, on the oil gelation efficiency are discussed. The results presented in this chapter have been submitted as Fereshte Damavandi, João B.P. Soares, *Evaluating the*

effectiveness of a new polymer organogelator for the solidification of oil spilled on water,
Langmuir, 2022

Chapter 5 provides a summary of investigations carried out in this work along with recommendations for future work on oil spill recovery.

Chapter 2: Polystyrene Magnetic Nanocomposite Blend: An Effective, Facile, and Economical Alternative in Oil Spill Removal Applications

Finding an efficient and economical method to remediate oil spills on water is a priority worldwide. In this article, we propose a solution to this problem using polystyrene magnetic nanocomposite blends composed of polystyrene chains grafted on the surface of silica coated on iron oxide nanoparticles and polystyrene. The hydrophobic and oleophilic magnetic polymer nanocomposite collected oil from the water surface quickly and efficiently. However, when the magnetic polymer nanocomposite was blended with polystyrene, the resulting material also absorbed oil efficiently from the water surface. The blending technique made it easier to prepare the absorbent and dramatically decreased its cost. These new absorbents absorbed oil up to 5 times their own weight in only 5 minutes. The excellent hydrophobicity, low density, and easy magnetic separation makes these new absorbents a promising alternative to recover oil from spilled in fresh and marine water.

2.1 Introduction

Oil spills are a major environmental concern worldwide. They may happen during exploration, transportation, and storage.[47] The scale of this problem is staggering, considering the global use of oil and petroleum products (10 million tones per day). For example, the Deepwater Horizon oil

spill accident in 2010 released 4.9 million barrels of oil in the Gulf of Mexico, severely damaging the environment and the economy.[48]

Although mechanical methods have been used for several decades to control oil spills, they suffer from major drawbacks. Oil booms create a boundary surrounding the spill and prevent it from spreading while skimmers collect the oil.[47] This first response, however, leaves behind a thin layer of oil residues (0.04 ~ 50 μm) on the water that threatens marine life.[18], [49] Although in situ burning can remove oil residues in the contained area, bad weather hampers its efficiency. Even in suitable conditions, burning produces gaseous combustion products and particulate matter. Dispersants are not promising either, since they break down the oil into small droplets that are even harder to collect.

Magnetic hydrophobic and oleophilic absorbents have been studied to overcome the limitations of traditional methods.[50]–[55] Magnetic sorbents are easy to separate from the water surface using an external magnet. Magnetic nanocomposite particles compete with other sorbents such as magnetic resins,[56], [57] nanofibers,[50] and foams.[58], [59] Although these oil sorbents are promising, they are difficult to collect, hard to recycle, expensive to use, and poorly selective.[10] Magnetic nanocomposite particles, on the other hand, are selective, smart, fast, small, light, and environmentally friendly.[60][52], [61]–[63]

Iron oxide nanoparticles (IONPs) have been widely used to prepare magnetic nanocomposites because of their low toxicity, low preparation cost, chemical stability, surface reactivity, and easy modification.[64]–[67] In addition, the porosity and hydrophobicity of iron oxide nanoparticles can be changed to increase oil recovery efficiency.[51], [68] For example, Zhu et al.[53] prepared porous core-shell Fe_2O_3 nanoparticles coated with a layer of carbon (7-36 nm) and modified with vinyltriethoxysilane to increase their hydrophobicity (the authors called this material $\text{Fe}_2\text{O}_3 @\text{C}$

nanoparticles). The superhydrophobic magnetic nanoparticles absorbed oil up to 3.8 times their weight, were stable, and could be recycled. Mirshahghassemi et al.[69] used polyvinylpyrrolidone-coated magnetic nanocomposites to treat the Deep Water Horizon oil spill from an oil-water mixtures, including pure water and synthetic seawater. They recovered 100 % of lower molecular mass alkanes (C₉-C₂₁) in 10 minutes and 67 % of C₂₂-C₂₅ alkanes in 40 minutes.[69]

Other studies have also shown that superparamagnetic IONP perform even better in practical oil spill clean-up applications because of their high magnetization and zero coercivity,[50], [56], [70] but their surfaces must be modified by coating with silica (SiO₂-IONP) or grafting polymer chains. Silica coating protects and stabilizes the IONP and provides the required surface chemistry for polymer grafting. Polymers with hydrophobicity and oleophilicity similar to polystyrene have been studied as low surface energy materials that absorb oil efficiently.[10] In addition to the hydrophobic affinity among oil molecules and polystyrene chains, most oils contain benzene rings that promote strong stacking interactions with the benzene rings in the polystyrene chains, increasing their oil absorption capacity. The high hydrophobicity and oleophilicity of polystyrene-grafted IONP nanocomposites combined with their fast magnetic separation capability make them excellent oil absorbers. [62], [48]

In this study, we first prepared dense hydrophobic polystyrene-grafted silica-coated IONP nanocomposite (PS-SiO₂-IONP) by surface-initiated atom transfer radical polymerization (SI-ATRP) (Figure 2.1) to recover oil from water. To the best our knowledge, this is the first time that SI-ATRP has been used to graft polystyrene chains onto the surface of silica-coated IONP (SiO₂-IONP) and the product has been used to remediate oil spills on water. We carefully chose SI-ATRP to bond the polystyrene chains via covalent bonds to the surface of SiO₂-IONP and increase their hydrophobicity and oil absorption capacity. [71] Then, we synthesized polystyrene chains by

reverse atom transfer radical polymerization (reverse ATRP). Finally, we blended the PS-SiO₂-IONP nanocomposite and polystyrene (PS/PS-SiO₂-IONP) to develop a simple and cost effective technique to remove oil from water. We believe this has also been the first time such blend has been made and used in oil spill remediation applications. Finally, the magnetic properties of the IONPs make it easy to remove the adsorbed oil from the water surface using a magnet.

The oil absorption capacity of the PS-SiO₂-IONP nanocomposite and the PS/PS-SiO₂-IONP blend were investigated by removing diesel and diluted bitumen spilled on water. The findings of this study demonstrate that this is an economical alternative material for large scale oil spill removal from the environment.

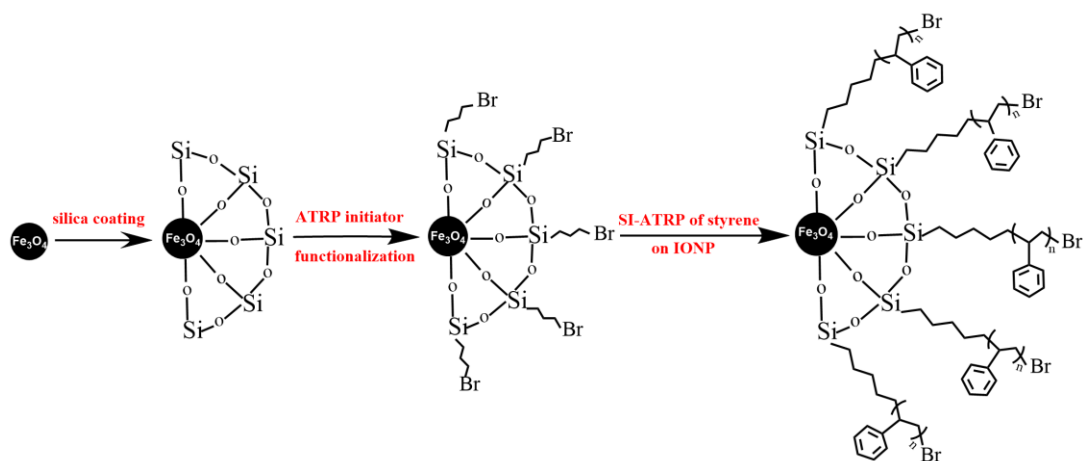


Figure 2.1 *Synthesis of PS-SiO₂-IONP nanocomposite.*

2.2 Material and Methods

2.2.1 Materials

Iron chloride (FeCl₃), sodium acetate (NaAc), tetraethyl orthosilicate (TEOS), (3-bromopropyl) trichlorosilane, ethylene glycol (EG), ethanol, 28% ammonium hydroxide, copper II bromide, 4,4-

Dinonyl-2, 2'-dipyridyl (dNbpy), tetrahydrofuran (THF), azobisisobutyronitrile (AIBN), toluene, and styrene were purchased from Sigma-Aldrich and used as received, unless noted otherwise.

2.2.2 Synthesis of Superparamagnetic Iron Oxide Nanoparticles, IONPs

Iron oxide nanoparticles (IONP) were synthesized by the solvothermal method, [72] with just slight changes in the synthesis time and iron precursor solution. In a typical procedure, an iron precursor solution was prepared by adding FeCl₃ (406 mg) and sodium acetate (1.026 mg) to EG (40 ml) at room temperature. Then, 1 ml of water was added to the mixture and the solution was stirred for 30 min under nitrogen atmosphere at 40 °C. The yellow mixture was then transferred to an autoclave chamber and heated for 8 h at 200 °C. The product was separated using a magnet bar (a permanent magnet with field strength of 5000 g at the pole), washed five times using water and ethanol, and dried in a freeze dryer overnight. Since we only could synthesize around 250 mg per each batch, we made several IONP batches to cover all the tests described in this manuscript.

2.2.3 Synthesis of SiO₂-IONP

The surface of the prepared magnetic IONP was coated with a silica shell to protect the iron oxide nanoparticles from further oxidation and to create a surface suitable for the next functionalization step. The Stöber method was used to coat the IONP with a silica shell. [73] First, 100 mg of IONPs were sonicated in ethanol and water solution (1:3 volume ratio) for 30 min to prepare 1 mg/mL suspension. Still under sonication, ammonium hydroxide (3 mL) and tetraethyl orthosilicate (139 mg) were added to the suspension. The mixture was stirred under nitrogen for 6 h. An external magnet was used to separate the SiO₂-IONP from the mixture. The silica-coated iron oxide nanoparticles were then dispersed and washed in ethanol under sonication. Finally, the black SiO₂-IONP were dried using a freeze dryer.

2.2.4 Functionalization of SiO₂-IONP with an ATRP Initiator (Br-SiO₂-IONP)

The ATRP initiator was grafted on the SiO₂-IONPs surface using a bromine-functionalized silane. In a 50 mL glass flask, 120 mg of SiO₂-IONP were suspended in 25 mL toluene under sonication for 30 min. Then, 5 mL of 4mM of (3-bromopropyl) trichlorosilane in toluene were added dropwise to the reaction flask. The reaction mixture was heated in a preheated oil bath at 110 °C for 24 h under continuous stirring. The resulting functionalized SiO₂-IONP was separated from the supernatant using a magnet bar and washed three times with toluene and THF to remove unreacted chemicals from the particle surfaces. The clean ATRP initiator-functionalized SiO₂-IONP (Br-SiO₂-IONP) was finally dried in a freeze dryer overnight.

2.2.5 Reverse ATRP of Styrene

Polystyrene was synthesized using reverse ATRP. In a typical polymerization, AIBN (28.2 mg), CuBr₂ (57 mg), and dNbpy (219 mg) were added to a 500 mL round-bottom flask equipped with a magnetic stirrer bar. A volume of 20 mL of styrene was passed through a column of aluminum oxide to remove the inhibitors. Then, 20 mL of toluene and styrene were added to the dry ingredients to make a solution. The homogenous solution was purged for 30 min under nitrogen flow and placed in a preheated oil bath at 70 °C. After 20 min, the green reaction mixture turned brown. The polymerization was allowed to proceed for different times to make polystyrene of different molecular weights at 110 °C, as shown in Table 2.1 below. The reaction mixture was left to cool down to room temperature and then precipitated with an excess amount of methanol.

Table 2.1 Polymerization conditions and polystyrene properties.

Sample	Time (h)	Measured M_n	D	Calculated M_n	Conversion (%)	$\ln([M_0]/[M])$
S1	2	12,300	1.36	11,447	11	0.17
S2	6	31,266	1.60	36,425	35	0.43
S3	12	81,501	1.40	78,112	75	1.37
S4	20	97,567	1.45	91,652	88	2.19

* $[M_0]$: initial monomer concentration, $[M]$: monomer concentration at a specific time

2.2.6 Synthesis of Polystyrene Grafts on Br-SiO₂-IONP (PS-SiO₂-IONP)

We carried out reverse ATRP (described in the previous section) and SI-ATRP simultaneously in the same reactor using the same catalyst complex to grow polystyrene grafts on the surface of Br-SiO₂-IONP. First, 120 mg of Br-SiO₂-IONP was dispersed in 10 mL of toluene with the aid of ultrasonication. The black mixture was then purged with nitrogen for 30 min and placed in a preheated oil bath at 110 °C (Reactor 1). Second, AIBN (28.2 mg), CuBr₂ (57 mg), and dNbpy (219 mg) were added to the 500 ml round bottom reactor containing 10 ml toluene and 20 ml styrene. The homogenous solution was purged for 30 min with nitrogen and placed in a preheated oil bath at 70 °C for 20 min (Reactor 2). Once the color of the contents of Reactor 2 changed from green to brown, the reaction mixture transferred to Reactor 1 for the rest of the reaction. The resulting black polystyrene-functionalized PS-SiO₂-IONP were collected with a magnet, washed three times with toluene and three times with THF to remove residues. The PS-SiO₂-IONP nanocomposites were dried overnight in a freeze dryer.

2.2.7 Nanocomposite Characterization

The size of the IONP was measured by dynamic light scattering (DLS) with a Malvern Zetasizer Nano-Zs using ethanol as dispersant. The magnetization measurements were performed by a Quantum Design 9T-PPMS dc magnetometer/ac susceptometer over the range of -30 to 30 KOe

at 25 °C. The morphology of nanoparticles was determined by field emission high-resolution scanning electron microscopy (SEM) on a Hitachi- S4800 HR at 30 kV and transmission electron microscopy JEOL TEM-2200FS imaging. Samples were prepared by dropping the nanoparticle suspension on a 400-mesh carbon grid and dried in a vacuum oven for 2 hours. X-ray powder diffraction (XRD) patterns were collected by a Rigaku XRD Ultima IV to study the products' structural properties. Fourier-transform infrared (FTIR) was carried out by FTIR (Agilent FTS 7000) in the range of 400-4000 cm^{-1} for the infrared characterization of the functionalized layer. X-ray photoelectron spectra (XPS) were acquired on a Kratos AXIS (Ultra) spectrometer with monochromatized Al $K\alpha$ radiation (1486.71 eV). The spectrometer was calibrated by the binding energy (84.0 eV) of Au 4f_{7/2} with reference to Fermi level. All peaks were referred to the signature C1s peak for adventitious carbon at 284.8 eV. Gel permeation chromatography (GPC) was carried out at 140 °C using a GPC unit (Polymer Char, Valencia, Spain) contained three linear columns filled with porous packing material (Agilent PLgel Olexis, 7.5×300 mm, 13 μm particles) and infrared (IR) detector and differential viscometer. GPC was calibrated using narrow molecular weight molecular distribution (MWD) polystyrene standards and the universal calibration curve. Thermogravimetric analysis (TGA) was performed in a nitrogen atmosphere at a heating rate of 10 °C/min from ambient temperature to 900 °C using TA TGA Q50.

2.2.8 Oil Absorption Experiments

Oil absorption experiments were performed by pouring a thin layer of oil on the top of the water. The oil absorption capacity was measured by adding a specific amount of absorbent on top of the oil layer. We tested one low-density oil (diesel) and one high-density oil (bitumen diluted in toluene). In a 1000 mL Pyrex dish, 500 mL of water was added following by 5 g of oil. Then, a specific amount of absorbent (M_1) was added to the Pyrex dish. After 5 min, absorbents and

absorbed oil were collected with a magnet bar and weighed (M_2). The oil absorption capacity was calculated by gravimetry using the formula $P = (M_2 - M_1) / M_1$. The absorption tests were performed at 23 °C. The samples were weighed using an analytical balance.

2.3 Result and Discussion

2.3.1 Synthesis and Characterization of PS-SiO₂-IONP

The IONP were synthesized by the solvothermal technique from an iron precursor at high temperature and high pressure in a suitable solvent. The average hydrodynamic diameter of the IONP was 700 ± 70 nm (Figure A. 1 in Appendix A). The size of the nanoparticles can be controlled by changing the reaction time and iron precursor concentration.[74] This is important because the magnetic properties of nanoparticles depend on their size: nanoparticles with the hydrodynamic size lower than 100 nm have superparamagnetic behavior.[66], [75] Since nanoparticles with superparamagnetic behavior have no magnetization remanence without an external magnetic field, they do not aggregate irreversibly due to magnetism residuals. Therefore, superparamagnetic nanomaterials with high magnetization as the core of the absorbent have a more robust magnetic response. The SEM image in Figure 2.2.a shows that uniform spherical nanoparticles were formed by clustering many much smaller nanoparticles (15-30 nm), which cause their superparamagnetic behavior.

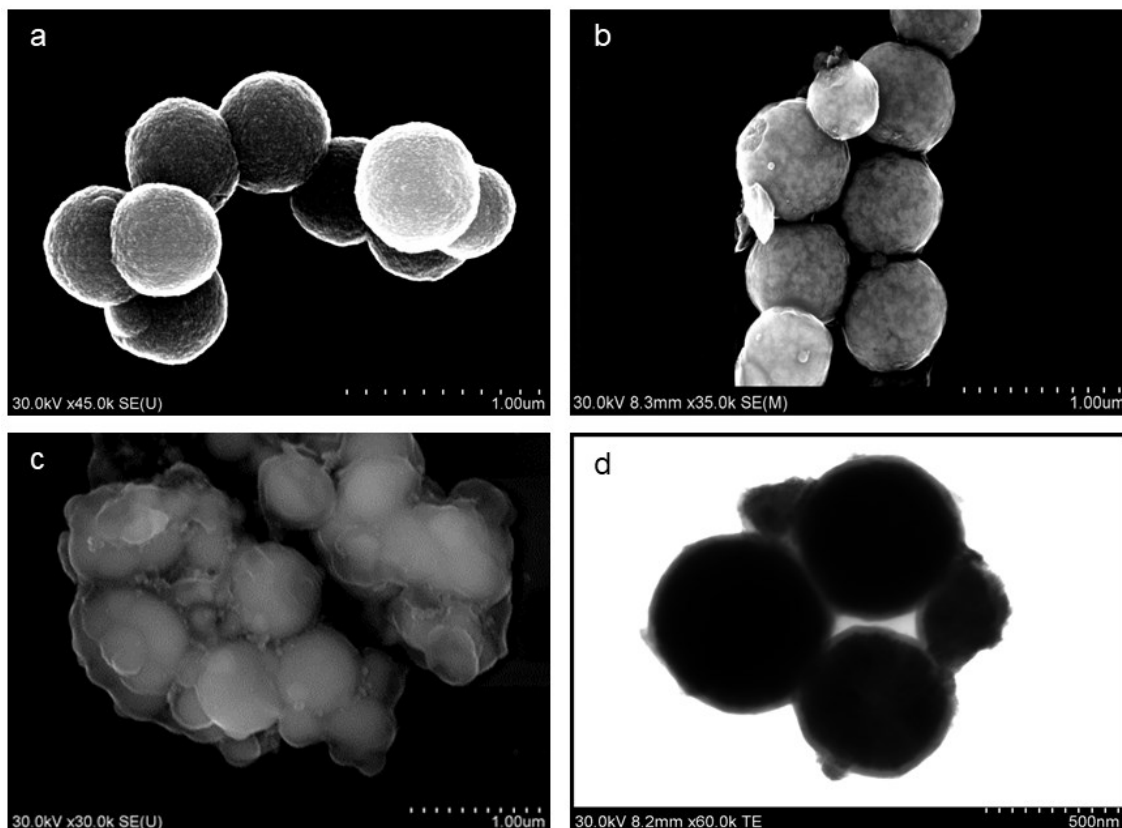


Figure 2.2 Micrographs of: a) IONP (SEM), b) SiO₂-IONP (SEM), c) PS-SiO₂-IONP (SEM), and d) SiO₂-IONP (TEM).

To test this assumption, the magnetic properties of the IONP were investigated by monitoring their responses to an external magnetic field. Figure A.2 in Appendix A shows the magnetic hysteresis loop of IONP at room temperature in the field range of ± 30000 Oe. The saturation magnetization of the IONP is 71 ± 5 emu/g, with no remanence and coercivity, which confirms they are superparamagnetic.

After successfully synthesizing the IONP, they were coated with a uniform silica shell (45 nm, measured by ImageJ), as shown in the SEM and TEM micrographs in Figure 2.2.b and Figure 2.2.c, respectively. Although the silica layer decreased the saturation magnetization of the IONP (Figure A.1.b in Appendix A), it preserved the IONP magnetic properties and ensured the IONP stability under harsh conditions. Moreover, the silanol groups on the surface of SiO₂-IONP

provided functional groups onto which the ATRP initiator could be attached by covalent bonds. We used (3-bromopropyl)trichlorosilane to functionalize the SiO₂-IONP surface with propyl-bromine as ATRP initiator. Then, styrene was polymerized using SI-ATRP, as explained in the experimental section. Figure 2.2.c is the SEM image of the PS-SiO₂-IONP after polymerization, showing a “cloudy” layer of polystyrene surrounding the SiO₂-IONP cores.

X-ray diffraction (XRD) was performed to study the crystal structure of the nanoparticles. Figure A.3.a in Appendix A shows six characteristic peaks at $2\theta = 30, 35.5, 43.1, 53.4, 56.9,$ and 62.5° , corresponding planes [220], [311], [400], [422], [511], and [440] of the cubic structure of Fe₃O₄ crystal. The spectra agree with those for Fe₃O₄ nanocrystallites reported in the literature.[76] Figure A.3 in Appendix A also shows that the same peaks are found in SiO₂-IONP, Br-SiO₂-IONP, and PS-SiO₂-IONP, confirming that the crystal structure of IONP was preserved during the preparation of the nanocomposite.

To verify whether or not the polystyrene grafting step was successful, we analysed the functional groups in IONP, SiO₂-IONP, Br-SiO₂-IONP and PS-SiO₂-IONP by FTIR (Figure A.4 in Appendix A). The characteristic bands at 572 cm^{-1} and 574 cm^{-1} , found in all spectra, are associated with the Fe-O bond of the magnetic core. Three characteristic adsorption peaks, 1060 cm^{-1} (Si-O stretching), 939 cm^{-1} (Si-OH bending), and 792 cm^{-1} (Si-O-Si bending) present in the spectra of SiO₂-IONP, Br-SiO₂-IONP, and PS-SiO₂-IONP confirms the existence of a silica shell on the surface of IONP in all materials[77]. It was not possible to detect the bromine group in Br-SiO₂-IONP by FTIR analysis, but we later used XPS analysis to confirm the success of the ATRP initiator functionalization step.

The peaks around 1440 cm^{-1} and 1600 cm^{-1} in Figure A.4.d in Appendix A are attributed to the C=C double bond stretching of the benzene ring of styrene molecules. The peaks at 2915 cm^{-1} and

3009 cm^{-1} in Figure A.4.d in Appendix A are due to the bending of $-\text{CH}_2-$ and aromatic C-H stretching of polystyrene chains, respectively.[78] Figure A.4.d in Appendix A shows that these peaks are only present in the PS-SiO₂-IONP spectrum, confirming the successful formation of polystyrene chains on the PS-SiO₂-IONP absorbent.

X-ray photoelectron spectroscopy (XPS) analysis was performed to investigate the chemical composition of each nanocomposite. Figure 2.3 shows the spectra for IONP, SiO₂-IONP, Br-SiO₂-SIONP, and PS-SiO₂-IONP. The peak assignments for each element is: Fe = 710 eV, O = 530 eV, C = 284.8 eV, Si = 104 eV, and Br = 70 eV.

Figure 2.3.a shows that the Fe2p peak of Fe appears in the XPS analysis of IONP. Figure 2.3.b, on the other hand, does not show a peak for Fe in the SiO₂-IONPs spectrum, confirming that a compact SiO₂ layer was formed around the IONP core. The appearance of peaks for Br3p (184 eV) and Br3d (70 eV) in Figure 2.3.c confirms that the ATRP initiator was attached to the SiO₂ surface in Br-SiO₂-IONP. Moreover, the characteristic signals for C-Si (283.8 eV), C-C and C-H (284.8 eV), and C-Br (286.3 eV) in the high resolution XPS scan of Br-SiO₂-IONP confirms the successful immobilization of propyl-bromine as the ATRP initiator (Figure 2.3.d).

In Figure 2.3.e, the presence of the strong binding energy peak of C1s (284.8 eV) shows a high fraction of C atoms in PS-SiO₂-IONP, as expected. More specifically, Figure 2.3.f shows that the binding energy for C1s of PS-SiO₂-IONP is only attributed to one peak, which represents the C-C and C-H bonds of polystyrene. In addition, no peak related to Br3d appears because the polystyrene grafts cover the Br groups on the surface of Br-SiO₂-IONP.

2.3.2 Synthesis of Polystyrene by Reverse ATRP

Instead of using alkyl halide initiators, such as those used in normal ATRP, reverse ATRP uses a conventional radical initiator such as AIBN. Reverse ATRP is easier to conduct because the catalyst

precursor in its higher oxidation state, such as Cu(II), is less sensitive to oxygen.[79] We used reverse ATRP to synthesize polystyrene in solution polymerization using AIBN (initiator), CuCl₂/dNbpy (catalyst complex), and toluene (solvent). After 20 min at 70 °C, the color of the reaction medium changed from light blue to brown, indicating that Cu had been reduced from Cu (II) to Cu (I). It also confirmed the thermal decomposition of AIBN and the formation of ATRP alkyl halide initiators. Polymerizations were carried out for 2, 6, 12, and 20 h. Table 2.1 compares the measured (by gel permeation chromatography) and calculated number-average molecular weights, M_n , dispersity (D), and conversions for each polymerization time.

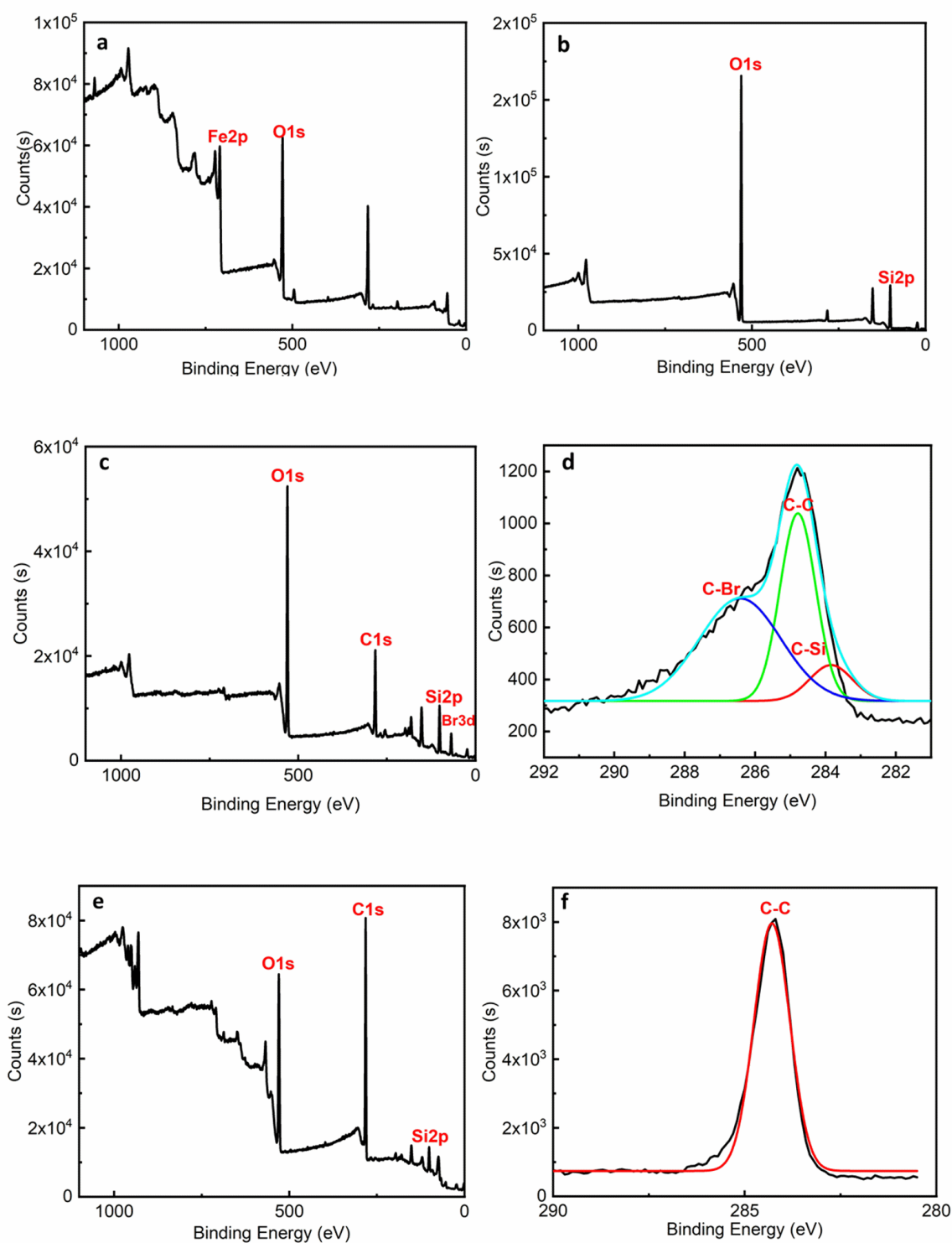


Figure 2.3 XPS spectra: a) IONP, b) SiO₂-IONP, c) Br-SiO₂-IONP, d) high-resolution XPS of carbon regions of Br-SiO₂-IONP, e) XPS spectra of PS-SiO₂-IONP, and f) high resolution XPS of carbon regions of PS-SiO₂-IONP.

The M_n values were calculated using the expression,

$$M_n = \frac{X[St]_0}{2[AIBN]_0} M_{St} \quad (1)$$

where X is monomer conversion, $[St]_0$ is the initial concentration of styrene, $[AIBN]_0$ is the initial concentration of AIBN, and M_{St} is the molar mass of styrene.

Figure 2.4.a shows that the measured and calculated M_n agree well and the M_n increases linearly with monomer conversion, as expected for controlled free radical polymerizations. Figure 2.4.b shows that the first-order kinetics plot of the polymerization is linear, indicating that the concentration of growing polymer chains remained constant during the polymerization,[80] confirming that polymer radicals and dormant species were in equilibrium from the beginning to the end of the polymerization.

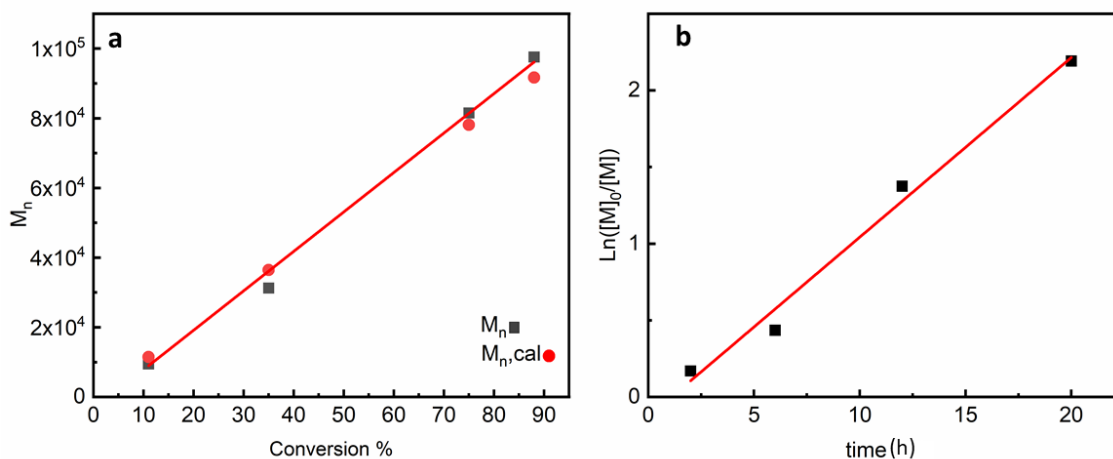


Figure 2.4 a) Dependence of number average molecular weight, M_n , on monomer conversion, b) polymerization kinetics plot for the reverse ATRP of styrene.

2.3.3 Synthesis of Polystyrene Grafts on Br-SiO₂-IONP by SI-ATRP

Conducting ATRP on the surface of Br-SiO₂-IONP allowed us to design the nanocomposite structure by controlling polymer molecular weight and graft density.[81] The previous section

showed that the reverse ATRP of styrene was carried out successfully with the Cu(II)/dNbpy catalyst complex. Therefore, we decided to use the alkyl halides produced during reverse ATRP as our ATRP initiators to control the SI-ATRP of styrene on the Br-SiO₂-IONP surface.

The reverse ATRP reaction mixture was kept at 70 °C for 20 min to ensure AIBN decomposed and converted to alkyl halide ATRP initiators. When the color of the reaction medium changed from light blue to brown (Cu(II) reduction to Cu (I)), the reaction mixture was added to the preheated Br-SiO₂-IONPs solution in toluene at 110 °C. It seems reasonable to assume that the styrene grafts formed on the surface of Br-SiO₂-IONP grow at the same rate as the polystyrene chains in solution. The polymerizations were run for 20 h to reach the maximum monomer conversion and to form PS-SiO₂-IONP with the longest polystyrene grafts.

The PS-SiO₂-IONP particles were separated from the reaction mixture using a magnet. Characterization tests, including SEM, FTIR, and XPS (see section Synthesis and Characterization of PS-SiO₂-IONP in Result and Discussion) confirmed that polystyrene was grafted on the surface of Br-SiO₂-IONP. This nanocomposite was also analysed by thermal gravimetric analysis (TGA) to quantify how much initiator and polystyrene were grafted on its surface.

Figure A.5 in Appendix A compares the TGA curves for SiO₂-IONP, Br-SiO₂-IONP, and PS-SiO₂-IONP, which showed an initial small mass loss at temperature below 200 °C due to the desorption of adsorbed water. At 400 °C, SiO₂-IONP, Br-SiO₂-IONP, and PS-SiO₂-IONP retained 93.39%, 92.43%, and 88.23% of their weight after the decomposition of the functional groups. Figure A.5.a in Appendix A shows that SiO₂-IONP retained 93.39 % of its weight at the 400 °C. We assumed that the weight loss was caused by the complete combustion of the ethoxy groups on the surface of the silica shell, while the difference in mass loss between SiO₂-IONP (93.39%) and Br-SiO₂-IONP (92.43 %) was due to the ATRP initiator coated on the surface of the latter. We applied the

same rationale to estimate the mass of polystyrene grafted on PS-SiO₂-IONP: The difference 88.23 % – 92.43 % accounts for the polystyrene grafts.

The ATRP initiator graft density and polymer graft density were calculated by using the equation,

$$\rho_g = \frac{\Delta w}{100 - \Delta w} \cdot \frac{\rho_p V_p N_A}{MS} \cdot 10^{-21} \quad (2)$$

where ρ_g is the grafting density in number of molecules per nm², Δw is the weight loss in each step, ρ_p is the density of the particles (2 g/cm³)[82], V_p is the volume of the particles calculated from a radius of 395 nm, N_A is Avogadro's number, M is the molar mass of thermally decomposed moiety, and S is the surface area of the particles calculated from a radius of 395 nm. The radius of 395 nm is the summation of the radius of IONP (350 nm) and the thickness of silica layer (45 nm). The ATRP initiator and polymers graft density were estimated to be 12.60 molecules/nm² and 0.07 chains/nm², respectively (see graft density calculation in the supplementary information). We substituted M with the GPC-measured M_n of the polymer, 97,567 g/mol, in our calculations.

2.3.4 Oil Absorption Performance

Oil absorption tests were conducted using 20 mg PS-SiO₂-IONP to absorb diesel and diluted bitumen (Figure 2.5.a). The magnetic properties of PS-SiO₂-IONP allowed it to be easily slid over the water surface to reach the oil-contaminated areas using a magnetic bar. It also made it easy to collect the oil-soaked PS-SiO₂-IONP seconds afterwards. The dependence of oil removal capacity on time was also studied to determine the time needed to reach the maximum oil absorption capacity.

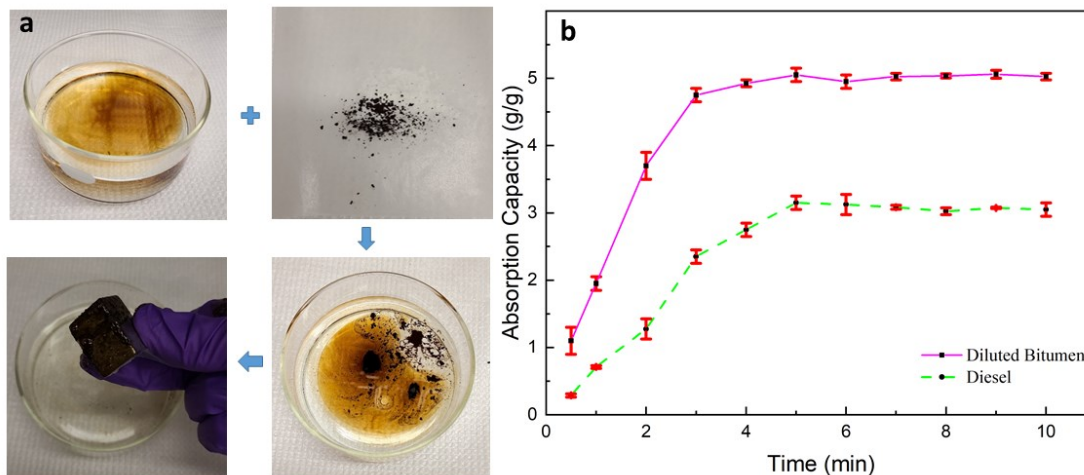


Figure 2.5 a) Photographs of diluted bitumen removal from the water surface with PS-SiO₂-IONP under a magnetic field and, b) oil absorption capacity of PS-SiO₂-IONP at different times for diesel and diluted bitumen.

Figure 2.5.b compares the oil absorption capacity of PS-SiO₂-IONP as a function of time. For diluted bitumen, the oil absorption capacity increased sharply and reached a plateau (5 g oil/g absorbent) after 5 minutes. The fast oil absorption is explained by van der Waals forces, hydrophobic effects, and stacking interactions between polystyrene molecules grafted on PS-SiO₂-IONP and the oil molecules.

A similar trend was observed for diesel removal. As expected, the absorption capacity is lower for diesel. Diesel's lower viscosity decreases the oil adherence onto the PS-SiO₂-IONP surface, which reduces the oil absorption efficiency. [83] Still, the performance is satisfactory, with a maximum capacity of 3 g diesel/g absorbent. Yu et al.[48] prepared Fe₃O₄/PS magnetic nanoparticles using emulsion polymerization to remove diesel from water surface. They reported that the highest absorption capacity belongs to the composite that could absorb diesel up to 2.495 times of its own weight. In other study, Chen et al.[62] showed that polystyrene-coated magnetic Fe₃O₄ nanocomposite (Fe₃O₄@PS) synthesised by emulsion polymerization could absorb lubricant oil up to 3 times of its own weight. However, lubricant oil has the lower viscosity than diesel, PS-SiO₂-

IONP nanocomposites could achieve the same oil (diesel) absorption capacity as $\text{Fe}_3\text{O}_4@\text{PS}$ nanocomposite. The high oil absorption capacity of PS-SiO₂-IONP nanocomposites for both low viscosity and high viscosity oils was mainly related to the covalently bonded PS chains on the surface of SiO₂-IONP using SI_ATRP. We intentionally used SI_ATRP polymerization method to grow PS chains with uniform lengths and high density resulting in high oil absorption capacity. In a second round of oil absorption tests, a series of PS/PS-SiO₂-IONP blends were compared. We tested different blending ratios and found out that the most effective PS/PS-SiO₂-IONP blends were achieved by mixing 20 mg PS-SiO₂-IONP with 200 mg of polystyrene with different molecular weights (Table A.1 in Appendix A). The polystyrene samples were milled using a small grinder to a fine powder and then manually mixed with PS-SiO₂-IONP (Figure 2.6.a). Oil removal experiments were conducted in a glass dish containing water and a thin layer of oil. We used a larger glass dish to provide the same oil thickness for higher amounts of oil.

The experiments were conducted for 5 min, and then the oil-absorbed on the PS/PS-SiO₂-IONP blend was removed using a magnet bar (Video 2 in the Supplementary Information). Figure 2.6.b compares the oil absorption capacity of these blends

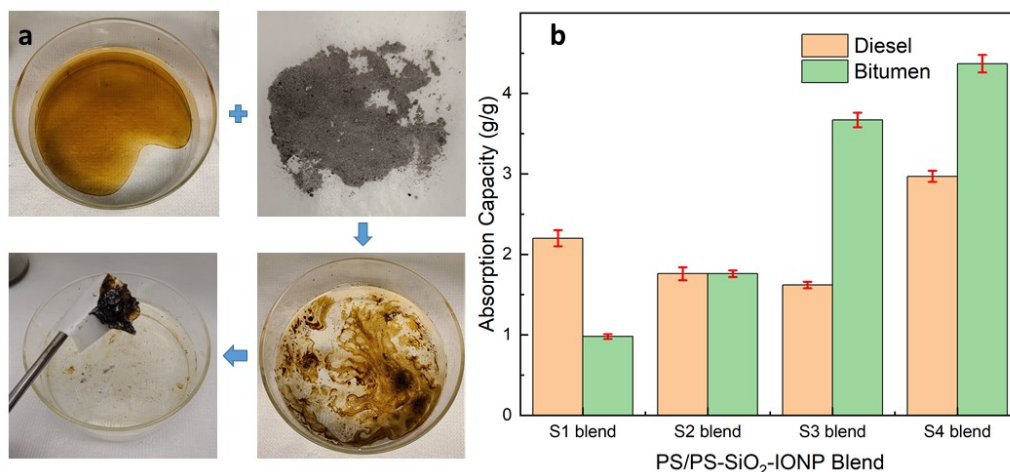


Figure 2.6 a) Photograph images of removal of diluted bitumen from the water surface by PS/PS-SiO₂-IONP blends under a magnetic field and b) oil absorption capacity of PS/PS-SiO₂-IONP blends for diesel and diluted bitumen after 5 min.

It is not surprising that the S4 blend (highest M_n) absorbed more oil than the other blends. With the same amount of polystyrene, the blend with the highest molecular weight polystyrene has more benzene rings connected by covalent bonds. Consequently, they form a more cohesive mass when oil interacts with the benzene rings via van der Waals and stacking molecular forces

All PS/PS-SiO₂-IONP blends with different polystyrene molecular weights remained floating on the surface of the water after the oil absorption because of its lower density. Moreover, the similar chemical structure of the ungrafted polystyrene chains and the polystyrene grafts in the PS/PS-SiO₂-IONP blends produced an oil-absorbed material that could be removed with a magnet bar without any fragmentation.

The two sets of oil absorption tests showed that PS/PS-SiO₂-IONP blend with a weight composition of 91% polystyrene and 9% PS-SiO₂-IONP nanocomposite had an oil absorption capacity equal to the pure PS-SiO₂-IONP nanocomposite. Therefore, the blending technique we are proposing can substitute more than 90 % of PS-SiO₂-IONP nanocomposite with polystyrene while still reaching the same oil absorption capacity, which is an economically attractive alternative, since it is more costly and time consuming to make the pure PS-SiO₂-IONP nanocomposite.

These novel absorbents seem to be a promising alternative to control oil spills because they do not sink even under heavy oil loadings, thus avoiding secondary environmental pollution, and can be easily collected applying an external magnetic field.

2.4 Conclusion

PS-SiO₂-IONP nanocomposites and PS/PS-SiO₂-IONP blends were successfully prepared and used to remove high- and low-viscosity oils from the water surface. The polystyrene chains grafted in the nanocomposites using SI-ATRP and added to the blends provided excellent hydrophobicity and oleophilicity, resulting in a high oil absorption capacity of up to 5 times its own weight in 5 minutes. The blending technique which substitutes more than 90% of PS-SiO₂-IONP nanocomposites with polystyrene has a considerable advantage in real field applications. Since they can be provided as powders, they can be easily spread over the contaminated water and removed with an external magnetic field. The combination of excellent hydrophobicity, buoyancy, environmentally friendliness, selectivity, and easy application, make these novel absorbents promising candidates for large-scale oil spill removal applications.

Chapter 3: Efficient Phase-Selective Powder Polymer

Organogelator for Oil Spill Remediation

Phase-selective organogelators that gels oil/water mixtures are useful to remediate oil spills on water. We designed and synthesized polymer organogelators, poly(styrene-*co*-10-undecenoic acid) with five different 10-undecenoic acid contents that could be added as powders at room temperature to gel oils with different viscosities. The morphologies and mechanical strengths of the gels were investigated using field-emission electron microscopy and rheological measurements, respectively. The gels formed porous fibrillar structures and had high stiffness. FTIR studies of these gels showed that hydrogen bonding and Van der Waals forces helped create 3D networks. The straightforward synthesis procedure, room temperature conditions, and easy powder delivery make poly(styrene-*co*-10-undecenoic acid) an attractive alternative to existing oil spill response methods.

3.1 Introduction

Most industrial processes and daily life activities depend on petroleum products. Unfortunately, oil spills may happen during production, transition, storage, and industrial applications.[1] For instance, the Exxon Valdez (1987) [84] and the Deepwater Horizon (2010) [85] oil spill accidents released 11 million gallons and 4.9 billion barrels of oil onto seawater, respectively. The adverse environmental impact and economic losses caused by oil spills have motivated academic, governmental, and industrial researchers to develop new remediation methods. When an oil spill happens, practical, fast, and effective methods are needed to prevent excessive environmental

damages.[86] Commonly used methods, such as skimmers and booms,[87] in situ burning,[88] dispersants,[89] sorbents,[10], [90] and bioremediation[91] are not efficient because they generate secondary air pollution and leave harmful chemical residues in the water.[92], [93]

Phase-selective organogelators (PSOG) have attracted significant interest over the last two decades. An organogelator is a compound that gels and immobilizes oil, preventing it from spreading. [94]–[96] Physical or supramolecular gels, contrarily to chemical gels, rely on non-covalent intermolecular interactions such as hydrogen bonding, hydrophobic interactions, π - π stacking, and van der Waals forces to form gels. Physical interactions between organogelator and oil molecules promote the self assembly of nano- or micro-scale networks that turn the oil into a gel.[97], [98]

Low molecular weight organogelators (LMWO) and polymers are the two main types of materials that can gel oil spills. LMWOs are typically amphiphilic compounds with molecular weights lower than 2000 Da which contain functional groups that help create molecular networks. Different LMWOs, such as sugar-based organogelators,[35] amino acids,[99] and alkane-derivatives,[100] ester-derivatives,[101] and urea-derivatives[102] have been used to clean up oil spills but they face some limitations. LMWOs usually require one or more synthesis and purification steps.[25], [103] Many of them must be dissolved in organic solvents because their powders dissolve too slowly in oil—leading to long gelation times[31], [104]—but most organic solvents can threaten aquatic life. Gels formed with LMWOs are also not stable long enough: they may crystalize and separate from the gel.[31], [35] These drawbacks limit the practical applications of LMWOs in field applications.[105]–[107]

Polymer organogelators, on the other hand, are promising because their entangled chains create 3D gel networks that entrap oil molecules.[108] When properly designed, polymers do not

crystallize and separate from the solution.[23] It is difficult for most common linear vinyl polymers to form gels in organic solvents and oils because they lack physical cross-linking points,[23] but some styrene and poly(methyl methacrylate) copolymers can generate 3D networks in organic solvents and form physical gels.[109], [110] Other macromolecular topologies, such as block copolymers,[111] hyperbranched polymers,[37] and polymer/cross-linking agent blends[29] have also been shown to form 3D networks in organic solvents, but their synthesis tends to be time-consuming and costly; their scale-up is also limited and laborious.

Industrial oil spill clean-up applications need an efficient, low-cost, and easy-to-make polymer organogelator that can form stable gels under different environmental conditions. Polystyrene is one the best polymer templates to make effective organogelators because: 1) the phenyl groups in their backbones may enforce the 3D networks through π - π stacking interactions, 2) the low cost and large-scale production of polystyrene makes it economically attractive for large scale applications, and 3) its high mechanical strength may make strong gels that can be easily removed from the water surface. However, polystyrene lacks physical crosslinking points and cannot form organogels by itself.

A few studies have tried to solve this limitation. Yu et al. [112] copolymerized 2-(((6-(6-methyl-4[1H]pyrimidionylureido)hexyl)carbamoyl)oxy)ethyl methacrylate (UPyEMA)—containing four hydrogen bonding groups—with styrene using reversible addition-fragmentation chain transfer (RAFT). The copolymers of (UPyEMA) and styrene formed stable gels in chloroform and 1,2-dichlorobenzene. Dasgupta et al.[113] blended oligo(*p*-phenylenevinylene) (OPV) and polystyrene with different tacticities to form organogels in several organic solvents such as benzene. They showed that OPV and polystyrene formed thermoreversible organogels with good mechanical properties.

In this work, we made a new polymer organogelator, poly(styrene-*co*-10-undecenoic acid) (PS10UA) and used it for oil spill recovery for the first time. The comonomer, 10-undecenoic acid (10UA), is a derivative of fatty acids composed of medium-length aliphatic chains (unsaturated) with a carboxylic acid group. These components may promote self assembly through van der Waals interactions and hydrogen bonding. 10-Undecenoic acid can be made by the pyrolysis of castor oil—a renewable biopolymer source.[114] The incorporation of 10-undecenoic acid in the polystyrene backbone also provides cross-linking sites that help form 3D networks. Moreover, poly(styrene-*co*-10-undecenoic acid) chain contain many phenyl groups that favor π - π stacking interactions and likely reinforce the aggregation of the gelator molecules into the network. We used the PS10UA powder to gel oils with low (diesel) and high (diluted bitumen) viscosities. A few LMWO powders have been used to gel diesel and crude oil, but they needed multiple synthesis steps and long gelation times.[36], [38], [40], [115] Interestingly, polymer organogelators dissolve faster and more easily than LMWOs in organic media.[23] To the best of our knowledge, the only other study that tested polymer organogelator powders was done by Nandi et al.[37] They investigated how hyperbranched polymeric organogelators—stearic acid-appended pendant *L*-aminoacid-based poly(methacrylate)—gelled organic hydrocarbons such as *n*-heptane, tetradecane, and diesel. They found that organogelators that could form gels using a heating/cooling cycle failed to form gels when they were added as powders. Our results, on the other hand, showed that the PS10UA organogelator powder could gel oils with both low and high viscosities.

3.2 Materials and Methods

3.2.1 Materials

Styrene, 10-undecenoic acid (10UA) (98 %), azobisisobutyronitrile (AIBN) (98%), methanol (99.8 %), and toluene anhydrous (99.8 %) were purchased from Sigma-Aldrich and used as received. Bitumen was recovered from an oil sands sample by Dean-Stark extraction over 24 hours. Diesel was purchased from a local gas station.

3.2.2 Characterization Techniques

Proton nuclear magnetic resonance ($^1\text{H NMR}$) was performed on a VNMRs 600 spectrometer to quantify the composition of poly(styrene-*co*-10-undecenoic acid). Deuterated chloroform was used as a solvent. All spectra were recorded at 400 MHz.

Attenuated total reflectance-Fourier-transform infrared (ATR-FTIR) spectroscopy was carried out in a FTIR instrument (Agilent FTS 7000) in the range of 400-4000 cm^{-1} . Xerogels (dried gels) were made by putting a freshly made gel on a piece of stainless-steel and drying it for 48 hours at room temperature in a vacuum oven. Before the data was collected, the xerogels and polymer powders were placed directly on the ATR crystal.

The gel structure was determined by field emission high-resolution scanning electron microscopy (SEM) on a Hitachi-S4800 HR microscope at 10 kV. A freshly prepared gel was attached to the coverslip and dried in a vacuum oven at room temperature overnight. It was then sputter-coated with a thin layer of gold before the electron microscopy analysis.

Gel permeation chromatography (GPC) was carried out at 140 °C using a high-temperature GPC unit (Polymer Char, Valencia, Spain) containing three linear columns (Agilent PLgel Olexis, 7.5×300 mm, 13 μm particles), an infrared (IR) detector, and a differential viscometer. The GPC

was calibrated using polystyrene standards with narrow molecular weight distribution and the universal calibration curve.

Rheological measurements were carried out on a TA Discovery HR-3 rheometer equipped with a steel parallel plate with a 40 mm diameter. The angular frequency sweep was performed at 25 °C at 1% fixed strain.

3.2.3 Copolymer Synthesis

Poly(styrene-*co*-10-undecenoic acid)—PS10UA—was made by free radical polymerization (Scheme 1 in Appendix B). Polymerizations were done in a 500 mL two-neck round-bottom flask equipped with a magnetic stirrer bar. A volume of 40 mL of styrene was passed through a column of aluminum oxide to remove the inhibitors. A specific amount of 10UA (the styrene/10UA molar ratios are listed in Table 3.1) and AIBN (43 mg, 263 μmol) were added to the mixture and purged for 30 min under nitrogen flow. The flask containing the mixture was sealed using a rubber septum and placed in a preheated oil bath at 90 °C. The polymerization was allowed to proceed for 2 h to make PS10UA of different molecular weights and copolymer compositions Table 3.1.

Table 3.1 Poly(styrene-*co*-10-undecenoic acid) with different copolymer compositions.

Sample	10-undecenoic acid/styrene feed ratio	^a Conversion %	^b Number average molecular weight, M_n	^c Dispersity (D)	^d 10-undecenoic acid composition (%)
PS	-	82	51 800	2.10	0
PS10UA-1	0.15	53	51 600	1.71	1.5
PS10UA-2	0.20	46	45 000	1.91	2.5
PS10UA-3	0.23	34	57 800	2.13	3.5
PS10UA-4	0.28	33	51 600	2.21	4.5
PS10UA-5	0.38	28	47 900	1.69	5.5

PS10UA-6	0.43	26	43 900	2.20	6.5
----------	------	----	--------	------	-----

^a Measured gravimetrically, ^b Measured by GPC, ^c $D = M_w / M_n$, ^d Measured using ¹H NMR

3.2.4 Minimum Gelation Concentration

The minimum gelation concentration is defined as the minimum amount of gelator required to gel an oil. We measured the minimum gelation concentration of PS10UA by pouring a thin layer of oil (100 μ L) on the top of water (20 mL in a 30 mL glass vial), and then gradually adding the PS10UA powder to the surface of the oil until it formed a gel. We tested one low-viscosity oil (diesel) and one high-viscosity oil (bitumen diluted in toluene, dilbit), as shown in Table 3.2.

The gel was considered to be completely formed when the gelled oil remained stable after the glass vial was shaken gently. Five minutes was the longest time it took for the least effective PS10UA sample gel the oil. Therefore, all the measurements were recorded after 5 minutes.

Table 3.2 Density and viscosity of diluted bitumen and diesel at 23 °C.

Oil sample	Viscosity (m Pa.s)	Density (g/ml)
Dilbit	118	0.98
Diesel	3.2	0.88

3.2.5 Oil Spill Removal Using Polymer Organogelators

The selective oil gelation experiments were performed in a 1000 mL Pyrex dish. First, a volume of 500 mL of aqueous NaCl solution (3.5 wt%) was added, followed by 10 mL of oil to form an oil/water mixture imitating an oil spill scenario. Finally, the organogelator powder was sprinkled over the oil layer. The process was considered complete when the gel could be moved on the water surface using a spatula.

3.2.6 Determination of Gel-to-Sol Transition Temperature (T_{g-s})

The thermal stability of dilbit and diesel gels prepared with different organogelators was measured by picking up the gelled oil from the water surface using a tweezer and placing it in a sealed vial. The vial was then immersed in an oil bath and heated gradually. The temperature at which the gel melted was recorded as T_{g-s}.

3.3 Result and Discussion

3.3.1 Copolymer Synthesis

Polystyrene and PS10UA samples were made by free radical polymerization under the conditions listed in Table 3.1. All polymers were characterized by ¹H-NMR and FTIR spectroscopy. The ¹H-NMR spectrum in Figure 3.1.A shows peak assignments of all functional groups in sample PS10UA-4. The copolymer composition was calculated by comparing the resonance signals at 6.6-7.5 ppm from aromatic H in styrene units with the aliphatic H shift at 2.3-2.37 ppm in the 10-undecenoic acid units (Figure B.1 in Appendix B). Even though the reactivity ratio towards 10-undecenoic acid copolymerization with styrene is small, we made copolymers with 10-undecenoic acid molar compositions varying from 1.5 to 6.5 mol % (Table 3.1) by increasing the 10-undecenoic acid fraction in the feed.

We also analyzed the copolymer with FTIR to confirm that the copolymerizations were successful. Figure 3.1.C shows the FTIR spectrum of the copolymer with the 6.5 mol % of 10-undecenoic acid. The absorption peaks at 3081, 3060, and 3022 cm⁻¹ correspond to aromatic C-H stretching vibrations, while the C-H asymmetric and symmetric stretching vibrations of the copolymer backbone appear at 2920 and 2850 cm⁻¹. The aromatic C=C stretching vibration peaks appear at 1600, 1492, and 1450 cm⁻¹, confirming the existence of benzene rings in the polymer structure.

The characteristic band at 1704 cm^{-1} arises from the C=O vibration of the carboxylic group in 10-undecenoic acid.

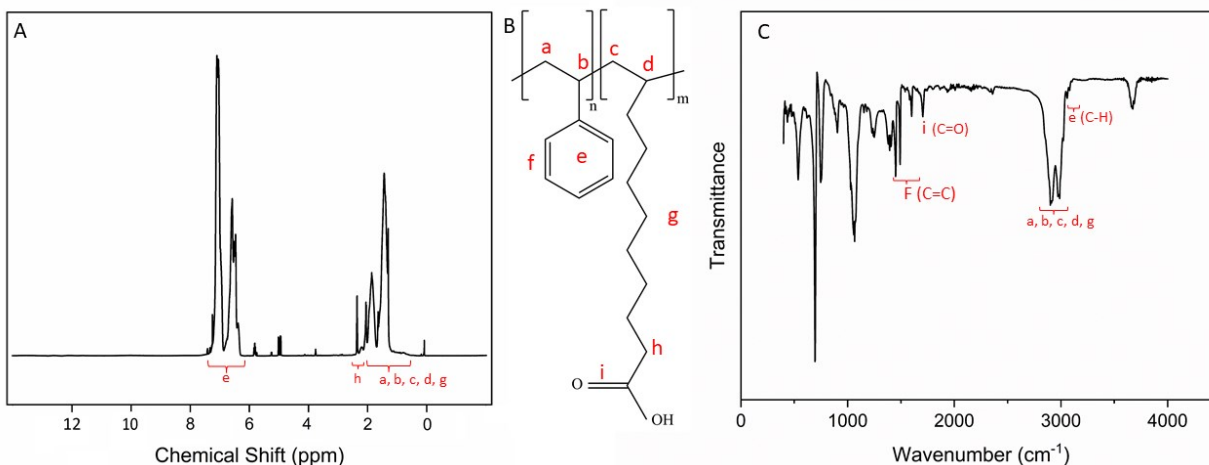


Figure 3.1 A) ¹H-NMR of sample PS10UA-4, B) Structure of PS10UA, C) FTIR spectrum of sample PS10UA-4.

3.3.2 Measuring the Minimum Gelation Concentration

In the vial inversion approach—the most common method for measuring the minimum gelation concentration—the gelator is first dissolved and heated to create a homogenous solution, then cooled down to form a gel. Since actual oil spills happen in large open-water environments, heating and cooling the organogelator/oil mixture cannot be scaled up to field applications. Instead, applying the organogelator as a powder to gel the oil on the water surface at room temperature simulates its performance in field applications more realistically.

Table 3.3 shows the minimum gelation concentration of each organogelator in dilbit and diesel, expressed as (mg of polymer)/(100 μL oil) \times 100. While polystyrene did not form gels in dilbit or diesel because it lacked physical cross-linking sites, all styrene/10-undecenoic acid copolymers gelled dilbit (Figure B.2 in Appendix B). Two of the gelators, PS10UA-3 and PS10UA-4, also gelled diesel, but needed higher minimum gelation concentrations than in dilbit. Although adding

hydrogen bonding groups to the organogelator increased the chance of self-assembly, its solubility in the oleophilic solvents and fuels decreased accordingly.

Table 3.3 Gelation properties of PS10UA in dilbit and diesel at room temperature

Sample	Minimum gelation concentration in diluted bitumen ^a	Minimum gelation concentration in diesel ^a
PS10UA-0	no gel	no gel
PS10UA-1	9.5	no gel
PS10UA-2	8	no gel
PS10UA-3	7	9.5
PS10UA-4	5.5	12
PS10UA-5	6	insoluble
PS10UA-6	7	insoluble

$$^a \text{ Minimum gelation concentration} = \frac{\text{mass of gelator (mg)}}{\text{volume of oil } (\mu\text{L})} \times 100$$

PS10UA samples with 10-undecenoic acid contents higher than 4.5 mol % were insoluble in diesel. Even though the organogelator absorbed the oil and swelled, it could not dissolve in it. We must face this compromise when designing new polymer organogelators: they must be able to dissolve in the oil phase, but they should also self-assemble to form cohesive 3D networks.[4]

3.3.3 Room-Temperature Phase-Selective Gelation

We discussed how PS10UA gelled dilbit and diesel in vials in the previous section. For a more realistic scenario, we scaled up the experiment and used a 3.5 wt% NaCl solution to mimic oil spills on the sea with two organogelator samples, PS10UA-3 and PS10UA-4. NaCl solutions have been used to simulate actual oil spills in previous publications.[27], [37], [104] Either dilbit or diesel was poured over the NaCl solution (Figure 3.2.a) to form a uniform layer of oil on the surface. Then, the organogelator (15 mg polymer/100 μL oil) was dispersed over the oil layer.

After 5 to 20 minutes, the powder dissolved completely in the oil (Figure 3.2.b) and formed a gel. Sample PS10UA-3 gelled dilbit in 8 minutes and diesel in 17 minutes, while sample PS10UA-4 gelled dilbit in 5 minutes and diesel in 20 minutes. The gel was removed and prepared for further characterization (Figure 3.2.c).

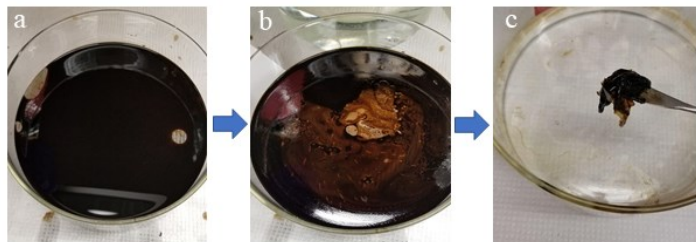


Figure 3.2 a) Dilbit layer on water, b) Dissolution of PS10UA powder in dilbit, c) Gel removal with a spatula.

Field applications need the gelled oil to be stable and strong, particularly on wavy seawater. The mechanical strength of the gels was measured in rheological experiments. Figure 3.3 shows the results of angular frequency sweep experiments carried at a constant strain of 1% for the dilbit and diesel gelled with PS10UA-3 and PS10UA-4 (15 mg polymer/100 μ L oil). The storage modulus, G' , is independent of the frequency and larger than the loss modulus, G'' , over a wide range of frequencies, showing the elastic response of the gels formed with PS10UA.[34] The large magnitude of G' (10^4 - 10^6 Pa) is comparable with chemically cross-linked gels, showing that the gels are stiff and strong, a requirement for stability in the choppy waters commonly encountered in oil spill recovery applications.[112], [116]

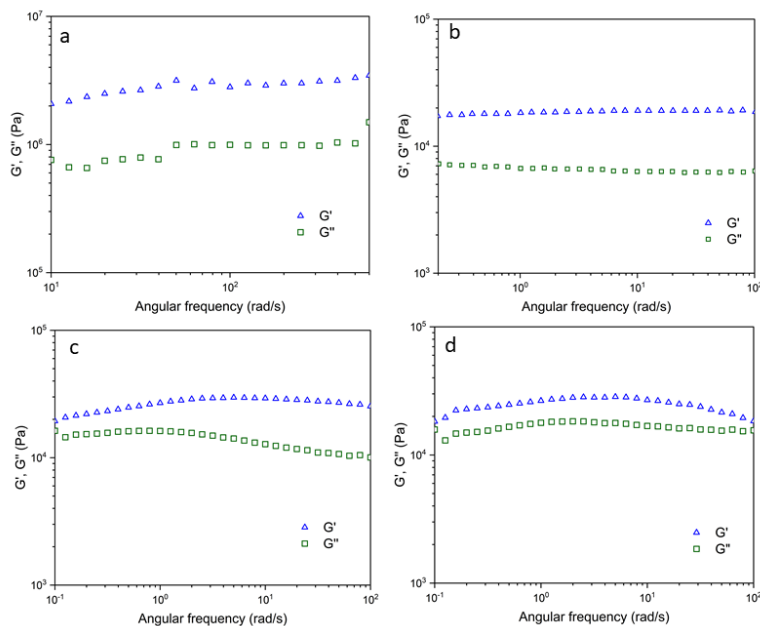


Figure 3.3 Dynamic rheology studies of: a) PS10UA-3 in dilbit, b) PS10UA-4 in dilbit, c) PS10UA-3 in diesel, d) PS10UA-4 in diesel. All experiments were done at a constant strain of 1 % and 15 mg polymer/100 μL oil.

The thermal stability of the gels was also investigated. The T_{g-s} for dilbit gelled with PS10UA-3 and PS10UA-4 were 57 °C and 65 °C, respectively. A smaller T_{g-s} indicates weaker intermolecular bonding between organogelator molecules and a weaker 3D structure. PS10UA-4 has higher cross-linking points, resulting in a gel with higher density that needs more energy to be dispersed. The type of the oil and its interaction with the organogelator molecules also affect the thermal stability of the gel. The T_{g-s} of gels in diesel with PS10UA-3 and PS10UA-4 were 45 °C and 40 °C, respectively. At the same concentration of organogelator, dilbit gels had higher T_{g-s} indicating stronger intermolecular interactions between organogelator and oil.[28]

The morphologies of the gels formed with PS10UA-3 and PS10UA-4 were also investigated via SEM. Figure 3.4 shows that the polymer molecules formed a porous and dense fibrillar 3D network. Figure 3.4.a, Figure 3.4.b, and Figure 3.4.d are top views of the gels, while Figure 3.4.c was taken from the edge of the torn gel to show the fibrillar morphology. The self-assembled

nano/micro fiber entanglements generate porous structures that absorb oil molecules and subsequently solidify them.

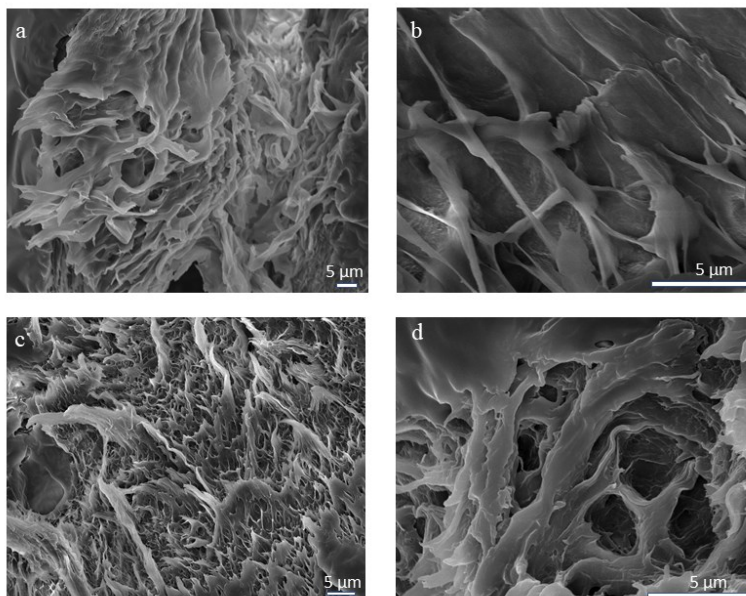


Figure 3.4 SEM images of dried dilbit gel formed with: a) PS10UA-3, top view, b) PS10UA-3, top view, c) PS10UA-4, edge, d) PS10UA-4, top view. All samples were formed using a ratio of 15% (w/v) organogelator to dilbit.

3.3.4 Gelation Mechanism

Three types of intermolecular interactions may promote gelation: 1) hydrogen bonding through functional groups, 2) van der Waals forces via long alkyl chains, and 3) π - π stacking interactions of aromatic groups (usually π -conjugated).[94], [117]

Since van der Waals forces and π - π stacking interactions are less prevalent in small molecules, hydrogen bonding plays a major role in gelation with LMWOs. The opposite happens with polymer organogelators, in which van der Waals forces and π - π stacking interactions are likely control the self-assembly of 3D structures. We analyzed PS10UA/diesel gels by FTIR to understand the gelation mechanism of our novel organogelators.

Figure 3.5 compares the FTIR spectra of PS10UA-3 (Figure 3.5.a) and PS10UA-3/diesel gel (Figure 3.5.b). The band at 1704 cm^{-1} is the C=O stretching frequency of the carboxylic acid groups in PS10UA-3, which shifts to lower frequencies ($1680 - 1700\text{ cm}^{-1}$) in the PS10UA-3/diesel gel due to the formation of hydrogen bonds.[118] The IR band at 3670 cm^{-1} in the PS10UA-3 corresponds to the O-H stretch vibration of the free carboxylic acid group, which broadens ($3020 - 3500\text{ cm}^{-1}$) due to hydrogen bonding in the PS10UA-3/diesel gel.[26] Figure 3.5.c shows that the PS10UA-4/diesel gel has a similar FTIR spectrum.

The peaks in the range of $2840 - 3000\text{ cm}^{-1}$ are the C-H asymmetric and symmetric stretching vibrations of the polymer backbone and alkyl side chains. Compared to the FTIR spectrum of PS10UA powder, the absorption peaks in the gels shifted to lower wavenumbers with higher intensities. This shift in peak location indicates that the polymer backbones and side chains of PS10UA self-assemble through Van der Waals forces.[37], [119]

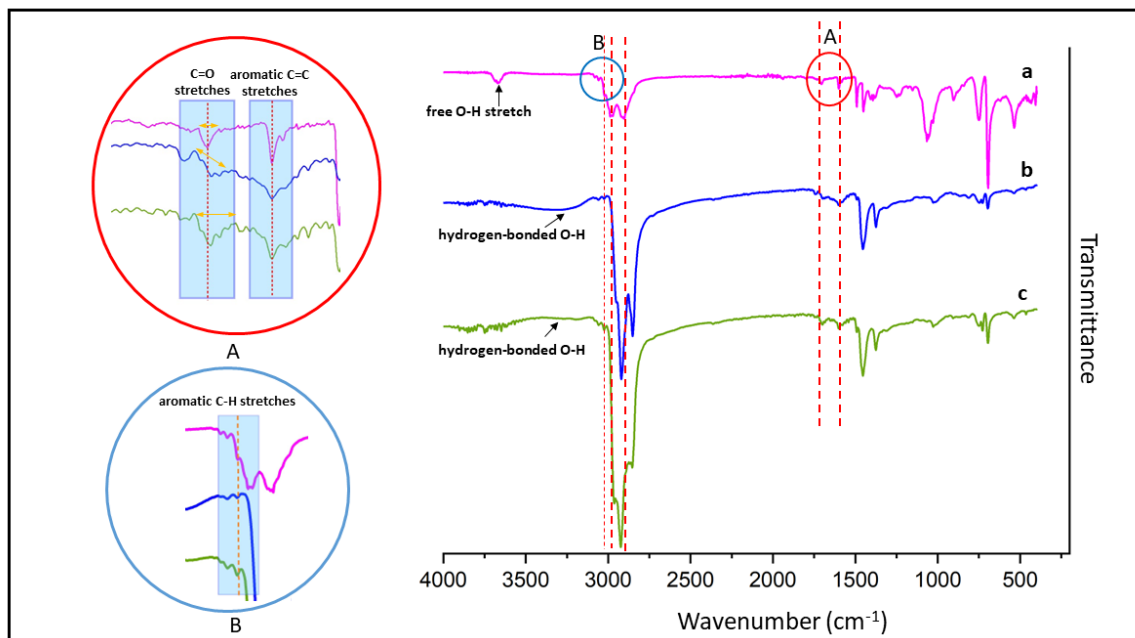


Figure 3.5 FTIR spectra of: a) PS10UA-3 powder, b) PS10UA-3/diesel gel, and c) PS10UA-4/diesel gel.

The characteristic bands at 1492 and 1600 cm^{-1} assigned to C=C stretching vibration and bands at 3081, 3056, and 3021 cm^{-1} assigned to aromatic C-H stretching vibrations, of benzene rings in the polymer backbone. No significant changes seem to have happened to C=C IR band after gelation, when we compare the benzene spectral bands in PS10UA-3 and PS10UA-3/diesel and PS10UA-4/diesel gels. However, the frequency of aromatic C-H at 3021 cm^{-1} shifted to a 3023 and 3025 cm^{-1} in PS10UA-3/diesel and PS10UA-4/diesel gels suggesting that the benzene rings participated in intermolecular π - π stacking interactions. [120], [121]

We assumed that the COOH groups in the 10-undecenoic acid monomer played an important role forming hydrogen bonds in the gel, since polystyrene alone could not gel dilbit or diesel. To further test this hypothesis, we made a similar polymer containing COOCH₃ instead of COOH groups. Figure B.3 in Appendix B compares the structures of poly(styrene-*co*-methyl-10-undecenoate)—PSM10U—and PS10UA. A sample of PSM10U containing 4 % of methyl-10-undecenoate and a $M_n = 56\,700$ g/mol could not gel the diesel spill (Figure B.4 in Appendix B) when added at a dosage of 15 mg polymer/100 μL oil, even though it could absorb the diesel (Figure B.5 in Appendix B). Since the PSM10U sample cannot gel diesel, it seems reasonable to assume that COOH groups are needed to make hydrogen bonds that affect self-assembly and physical cross-linking of PS10UA during gelation.[27]

The unsuccessful gelation tests with polystyrene (Table 3.3) and PSM10U show that hydrogen bonding is needed to gel diesel. While the aromatic rings in the PS10UA backbones are likely to promote π - π stacking interactions and help form the PS10UA/diesel fibrillar structure, the mobile 10-undecenoic acid side chains are essential to create physical cross-linking sites through hydrogen bonding and produce gels with high mechanical strength. Figure 3.6 proposes a tentative scheme for this gelation mechanism.

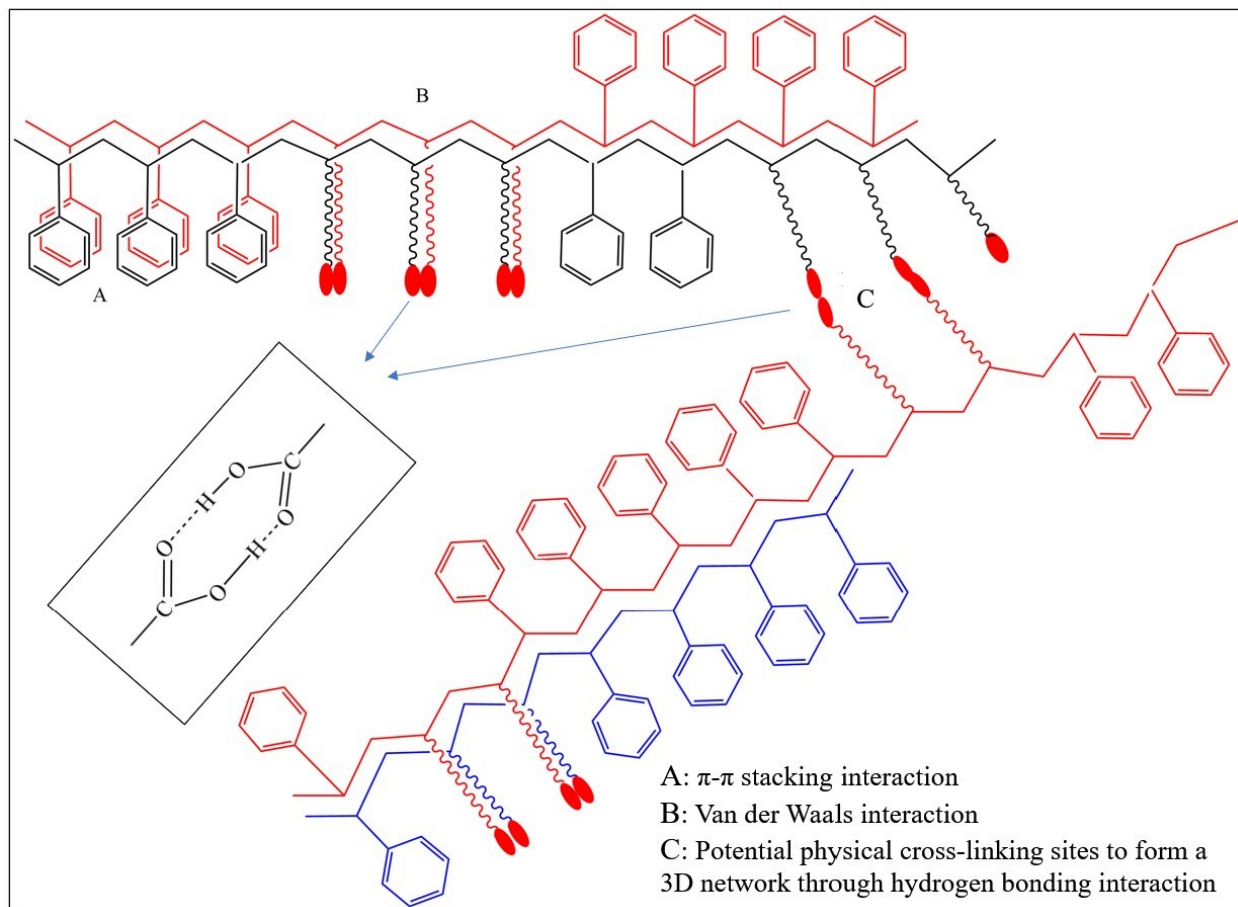


Figure 3.6 Tentative gelation mechanism of PS10UA.

It is interesting to consider whether the oil trapped in this 3D network could be recovered and whether the organogelator could be recycled. More volatile oils, such as diesel, could be separated from the organogelator by distillation; non-volatile oils, such as bitumen and crude oil, would require solvent extraction followed by distillation to separate the extracted oil from the solvent. Although technically feasible, it is likely that these unit operations would be too costly on an industrial scale. In addition, the PS10UA organogelators—being mainly composed of polystyrene and a few alkyl chains—are too inexpensive to justify recycling costs. It is likely that the gelled oil produced by PS10UA (itself mainly composed of C and H atoms) could be returned directly to a regular oil-refining process for further processing as a low-grade oil.

3.4 Conclusions

We designed and synthesized a series of poly(styrene-*co*-10-undecenoic acid)—PS10UA—organogelators using free radical polymerization. These novel polymers can gel mixtures of dilbit/water and diesel/water. The gelling abilities of the novel PS10UA organogelators were investigated with low (diesel) and high (diluted bitumen) viscosity oils, showing that their gelation performance was influenced by comonomer composition and oil viscosity. PS10UA also gelled oil in the presence of simulated seawater, making gels with high mechanical strengths and stiffness thanks to the highly porous morphology of the 3D network they formed.

Easy polymer synthesis, facile powder application, high gelation ability, phase-selectivity, high oil uptake, strong gel structure, and possible oil and organogelator recovery make poly(styrene-*co*-10-undecenoic acid) a promising alternative to remediate oil spills in water.

Chapter 4: Evaluating the Effectiveness of a New Polymer Organogelator for the Solidification of Oil Spill on Water

Solidifiers turn oil slicks into cohesive agglomerates, providing a simple method to remediate oil spills. Their efficiency depends on their physical and chemical properties and on field conditions. We investigated how poly(styrene-*co*-10-undecenoic acid) solidified diluted bitumen spilled on artificial seawater as a function of solidifier:oil ratio, contact time, and solidifier particle size. Poly(styrene-*co*-10-undecanoic acid) turned the oil layer into a cohesive mass at a solidifier:oil ratio of 1:8 after 15 minutes. Smaller solidifier particles with higher bulk densities also solidified oil spills more efficiently. Evaluating the effectiveness of polymer organogelators is essential to develop a comprehensive solidification testing protocol.

4.1 Introduction

Oil solidifiers were introduced in the sixties as means to recover oil from contaminated areas and prevent it from spreading. [22] Solidifiers change oils from liquids to solids or semi-solids that are easier to remove from the environment. The solidification mechanism depends on how the solidifier interacts with the oil molecules. [122] Polymer sorbents and polymer gelators solidify oil through physical interactions – such as van der Waals forces – without forming covalent bonds. [123] [23] Unfortunately, the lack of standards for their use under different environmental conditions has limited their widespread adoption. [124]

The efficiency of a solidifier is quantified by how much of it is needed to solidify oil under a set of conditions. Parameters such as oil composition, viscosity, and layer thickness, oil/solidifier

contact time, solidifier bulk density, and medium temperature influence their effectiveness. Field and laboratory tests have studied how these parameters affect oil solidification. Fingas et al.[125] showed that percentages of solidifier ranging from 16 % to over 200 wt. % were needed for effective solidification. The authors developed a standard method to test the efficiency of solidifiers by adding them – at 1 minute intervals – to oil spills under continuous stirring until the oil appeared to be solidified. The best solidifier was tested larger scale by the Canadian Coast Guard and the Canadian oil industry. Twice as much solidifier was needed in the field than in the laboratory. [126] Ghalambor [20] compared the performance of 23 oil solidifiers with three crude oils under static and dynamic (200-400 ppm) conditions for 30 minutes. He found that their efficiency depended on the type of the crude oil, which may have wide molecular size distributions and different chemical compositions.[127] DeLaune et al.[124] used the commercial solidifier Nochare A650 to remove South Louisiana crude oil near the shore. The test was carried out for four days with a solidifier:oil (SOR) ratio of 1:2. Nochare A650 solidified over 70 % of the oil, forming a rubber-like mass that could be removed by mechanical methods. [124] Rosales et al. used five solidifiers to remove Prudhoe Bay crude oil from artificial seawater in the laboratory as a function of solidifier/oil contact time, SOR, water volume, and solidifier surface area. A SOR = 1:4 solidified crude oil from 58 % to 84 % in 30 minutes. Increasing the contact time improved the efficiency slightly. [128] Sundaravadivelu et al. investigated the effect of SOR, mixing energy, water salinity, and beaker size on the performance of five commercial solidifiers, using an ultraviolet-visible spectrometer to measure how much oil remained on the water surface after removing the solidified product. The only statistically significant parameters were solidifier type and SOR. [46]

Although the exact structures were not disclosed, most of the reported commercial solidifiers contained polymer sorbents alone or combined with cross-linking agents. Knowing the physical and chemical properties of these materials is essential because they determine the solidification mechanism which, in turn, affects the solidification efficiency. [129] The consistency and cohesiveness of the final product also depends on the solidifier properties.

Organogelators are a recent category of oil solidifiers. Their solidification mechanism can be divided into three steps: 1) dissolution of the organogelator in oil, 2) formation of a 3D network through intermolecular forces among the organogelator molecules, and 3) entrapment of the oil molecules into the 3D network and formation of a cohesive gel. [118] No studies have been reported on the efficiency of polymer organogelators as solidifiers of oil spills. In this article, we quantified the performance of poly(styrene-*co*-10-undecenoic acid) as an organogelator solidifier for the removal of diluted bitumen from the surface of artificial seawater as a function of SOR, oil/solidifier contact time, and solidifier particle size. This study adds valuable information to the protocol to test the effectiveness of organogelators.

4.2 Materials and Methods

We made a new polymeric organic solidifier, poly(styrene-*co*-10-undecenoic acid), in our laboratory and applied it as a solidifier to remove dilute bitumen (dilbit) from artificial seawater (an aqueous 3 wt% NaCl solution).[104] Bitumen was recovered from a rich oil sands grade by Dean-Stark extraction over 24 hours and diluted using toluene to make dilbit. The viscosity and density of the dilbit were 14 m Pa.s and 0.97 g/ml, respectively. Toluene was purchased from

Sigma-Aldrich and used as received. The solidifier, produced as a white rigid polymer mass, was milled using a small grinder (Figure C.1 in Appendix C) and used with or without sieving.

4.3 Experimental Procedure

We did all experiments in a petri dish by adding 1 mL of dilbit to 20 mL of artificial seawater using SORs of 1:32, 1:16, 1:8, 1:4, 1:2, and 1:1 to find the ratio needed to turn the oil slick into a agglomerate that could be removed from the water surface with a spatula. We added the solidifier to the oils slick for 15, 30, 60, and 120 min to study the effect of contact time on solidification efficiency. We also sieved the solidifier powder in a Grainger motorized sieve shaker (ASTM C136, Figure C.2 in Appendix C) using mesh sizes of 1000, 850, 500, 250, and 45 μm to study the effect of the solidifier particle size on oil solidification.

4.4 Result and Discussion

4.4.1 Effect of Solid-to-Oil Ratio (SOR)

Figure 4.1 shows the effect of SOR on the solidification of dilbit with our new organogelator. All experiments lasted for 30 minutes, the contact time suggested in the literature. The amount of solidifier was not enough to cover the entire oil surface for $\text{SOR} < 1:8$: it could only solidify a few isolated oil domains, while the rest of the oil slick remained liquid (Figure 4.1.a). Figure 4.1.b shows that poly(styrene-*co*-10-undecenoic acid) solidified most of the oil when $\text{SOR} \geq 1:8$. The pictures in Figure 4.1.c were taken after we collected (but not removed it from the water surface) the solidified oil with a spatula: the liquid oil changed into an agglomerate without leaving any oil

on the water surface. The excess solidifier (white powder), whenever present, did not interfere with the oil solidification.

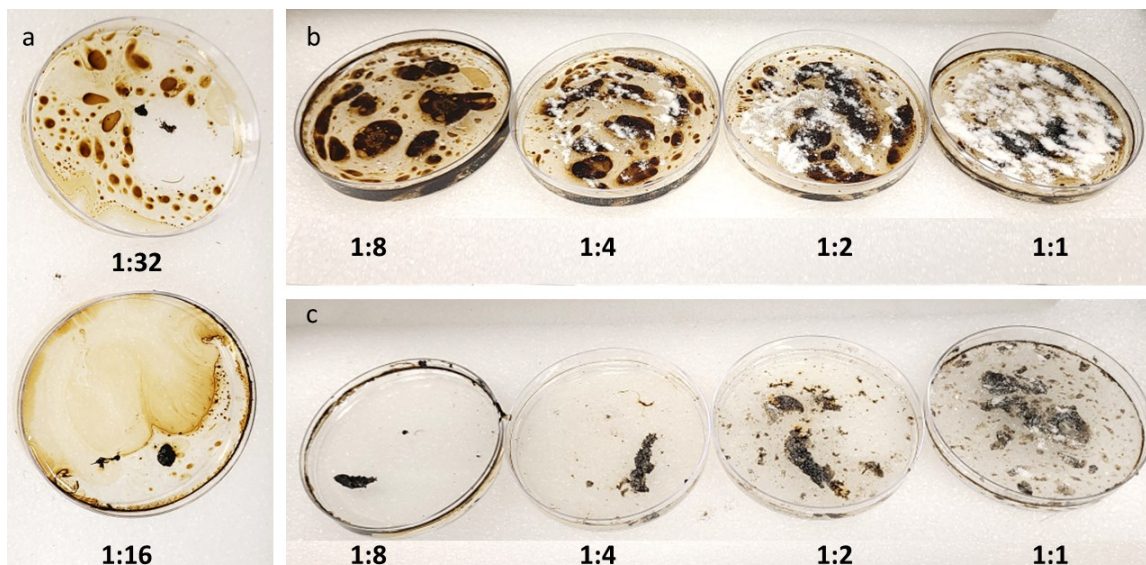


Figure 4.1 Dilbit solidification with poly(styrene-co-10-undecenoic acid) at different solidifier-to-oil ratios: a) 1:32 and 1:16, b) 1:8, 1:4, 1:2, and 1:1, c) 1:8, 1:4, 1:2, and 1:1, solidified oil collected with a spatula. Contact time = 30 min.

4.4.2 Effect of Oil and Solidifier Contact Time

The solidifier/oil contact time is a critical parameter in oil remediation procedures. If the oil and the solidifier interact too fast, the solidifier will make a crust on the surface of the oil slick that may prevent it from interacting with the rest of the oil spill. Contrarily, a too slow interaction will render the solidifier unusable. [22] Some researchers suggested the adoption of predetermined endpoints when evaluating the effectiveness of solidifiers, [128], [130] but endpoints may underestimate the performance of adequate solidifiers while overestimating the effectiveness of others with lower performance relative to SOR. [122] Therefore, a better approach is to measure the minimum contact time the solidifier needs to make the oil cohesive enough to be removed from the water surface. Unfortunately, the methods recommended to compare the efficiency of solidifiers ignore the consistency and cohesiveness of the final products and only report the

endpoint. This may be acceptable for commercial solidifiers that rely on absorption as their main solidification mechanism. However, it may not apply to solidifiers, such as polymer organogelators, that work with a different mechanism.

Four different contact times (15, 30, 60, 120 minutes) were compared, setting SOR = 1:8. We measured the minimum contact time our solidifier needed to gel the dilbit by checking the Petri dishes every 5 minutes to find whether the gel had acceptable cohesiveness. Figure 4.2.a illustrates four replicates after 5 min, showing that the solidifier needed more time to be completely dissolved in the oil. Figure 4.2.b shows that after 15 min, the oil solidified enough to be moved on the water surface with a spatula without breaking apart. However, because of the non-uniform sprinkling of the solidifier powder, very little oil remained intact at the end of the experiment. Even though 15 minutes was determined as the minimum contact time, we continued the rest of the experiments to the end of the assigned contact time. As Figure 4.2.b shows, the cohesiveness and strength of the solidified oil after 30 minutes is better than after 15 minutes. We observed the same trend for 60 and 120 min, Figure 4.2.c. The solidified oil after 120 min had the highest mechanical strength and cohesiveness. After a contact time of 3 h, the mat-like gelled oil could be picked up with a tweezer (see Figure C.3 in Appendix C).

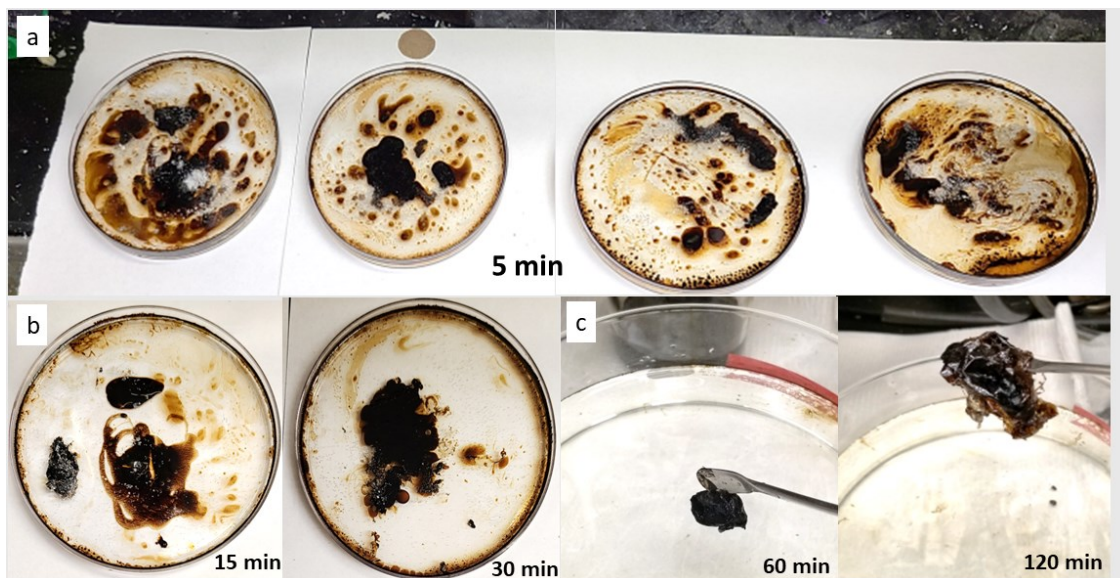


Figure 4.2 Effect of solidifier and oil contact time: a) 5 min, b) 15 and 30 min, c) 60 and 120 min (because some of the oil adhered to the walls of the petri dish, we repeated the 60 and 120 min tests in a 1000 ml Pyrex dish). SOR = 1:8.

4.4.3 Effect of Solidifier Powder Size and Bulk Density

We studied the effect of POS particle size (which correlates with bulk density) on oil removal efficiency by treating dilbit with POS samples having five different powder sizes/bulk densities, SOR = 1:8, and contact time of 15 min. Table 4.1 shows the relation between bulk density and particle size for these samples and Figure 4.3 depicts their shapes.

Table 4.1 Particle sizes (p.s.) and bulk densities of POS samples.

Particle size (μm)	1000 < p.s.	850 < p.s.< 1000	500 < p.s.< 850	250 < p.s.< 500	45 < p.s.< 250	p.s.< 45
Bulk density (g/cm^3)	0.36	0.42	0.47	0.51	0.57	0.69

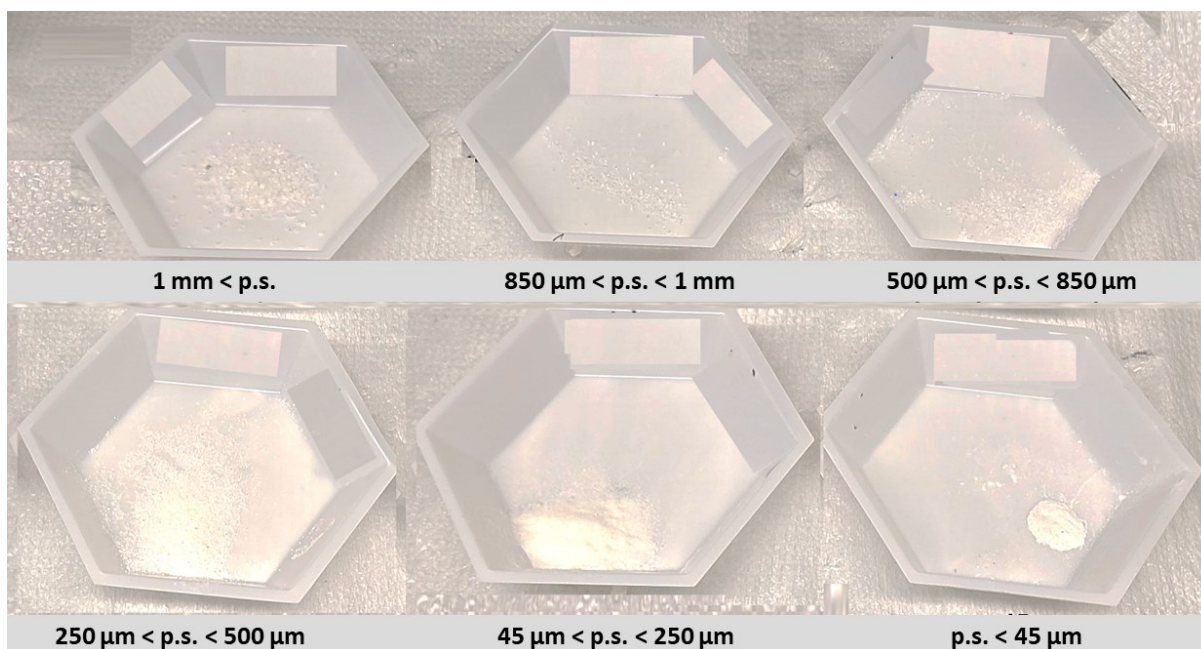


Figure 4.3 POS samples with different particle sizes (p.s.) after passing through the mechanical shaker machine.

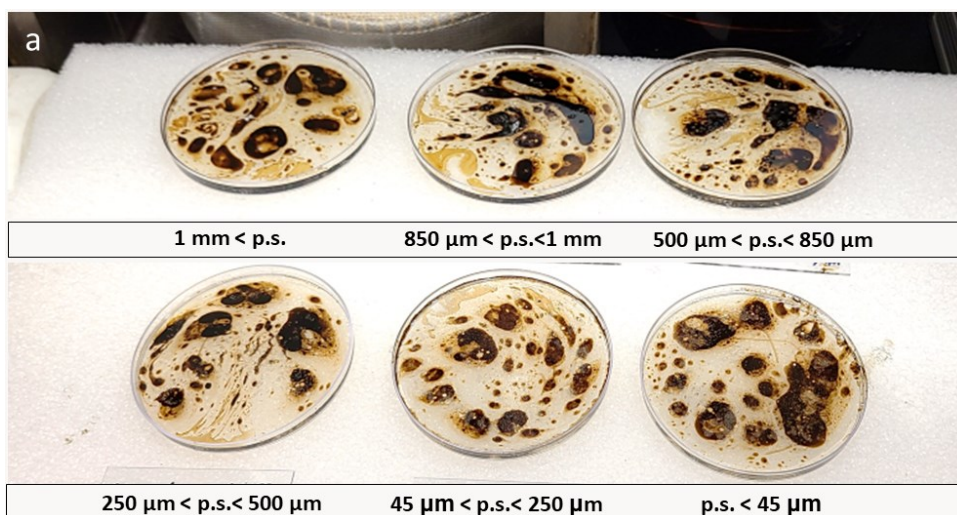
Figure 4.4.a illustrates that the POS particle size affect its ability to solidify the oil slick. The best performance—no liquid oil left at the end of the experiment—was reached with finest POS particles ($< 45 \mu$), while the worst was with the coarser POS particles ($> 1 \text{ mm}$). Figure 4.4.b shows that after the solid oil was collected with a spatula, the mass of oil left over on the water surface increased steadily from the largest to the smallest POS particle sizes, showing that the oil solidification efficiency increased with the increase in POS bulk density.

The results of our experiments disagree with the Sundaravadivelu et al., report, concluding that commercial polymer solidifiers with lower bulk density were more efficient. They studied the influence of the properties of 12 different commercial solidifiers on oil removal efficiency and concluded that the effectiveness of the solidifiers depended on the physical properties such as bulk density and pore size.[129]

The effect of the bulk powder density on the solidifier performance mainly depends on the solidification mechanism. If physical sorption is the dominant mechanism, the lower the bulk

density, the higher the free volume available for oil sorption resulting in higher oil removal efficiency. [129][131]

In case of organogelator solidifiers such as PSO, initial higher oil absorption helps with the dissolution. Because organogelators first dissolve in the oil to start the gelation, the dissolution step play an important role in the gelator's oil removal performance. Smaller particles (higher bulk density) dissolve in oil (faster dissolution) and form 3D gel structures more quickly, while larger particles take longer to do so. Besides, the distribution of the powder particles on the oil surface may also affect the oil removal efficiency. Organogelator particles with the smaller sizes, could more uniformly spread all over the oil surface. Larger oil/organogelator contact surface would result in higher organogelator dissolution leading to a higher solidification efficiency.



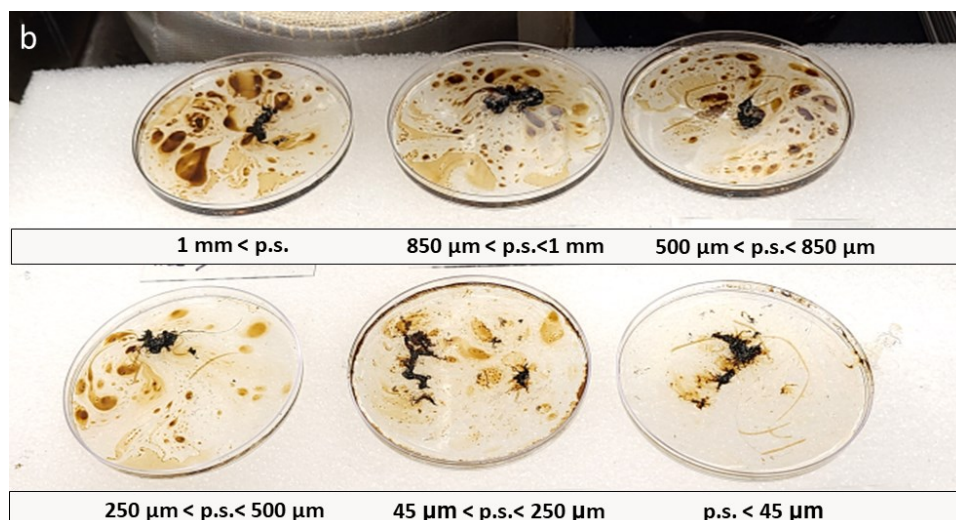


Figure 4.4 a) Oil removal experiments of Dilbit using POS with different particle size, SOR = 1:8, 15 min; b) Final solid oil collected using a spatula, SOR of 1:8, 15 min.

4.5 Conclusion

The solidification effectiveness of a polymer organogelator solidifier (POS) was studied as a function of operational parameters (SOR and oil/solidifier contact time) and solidifier bulk density. POS at SOR of 1:8, which is 2 times lower than the currently proposed SOR in the literature, completely solidified dilbit. A contact time of 15 min was enough to reach a cohesive solidified oil but extending the contact time increased the solidified oil's cohesiveness and consistency, which is promising for field applications. Higher bulk density POS samples performed the best, dissimilar to the common commercial polymer solidifiers.

This preliminary laboratory study of polymer organogelator solidifier's effectiveness showed that, for the further standard protocol establishment, the solidifier's mechanism of action should be considered as crucial as the operational parameters.

Chapter 5: Conclusions and Recommendations

5.1 Conclusions

The main objective of this thesis was to remediate oil spills relying on polymer science and nanotechnology. I selected nanocomposites and polystyrene copolymers because they are highly porous, and have the required hydrophobic/oleophobic balance. Compared with most other polymers, making polystyrene is cheaper, making it easier to scale up to large-scale oil spill remediation conditions.

In my first investigation, I used magnetic polystyrene nanocomposites as an oil solidifiers to remove high (diluted bitumen) and low (diesel) viscosity oil from the water surface. The magnetic polystyrene iron oxide nanocomposites solidified oil very fast, 5 times its weight in 5 minutes. The solidified oil was also easily removed from the water surface using a magnet. More interestingly, I observed that the oil absorption was selective, and the absorbed oil floated on the water surface. In the next step, I replaced 90 % weight of the magnetic polystyrene nanocomposite with pure polystyrene, and noticed that the oil absorption efficiency remained the same. This technique reduced the preparation steps and significantly decreased the cost while achieving the desired performance.

I also developed a novel polystyrene copolymer that worked as an organogelator to solidify oil spills. I copolymerized styrene with 10-undecenoic acid to add the required organogelation functionality to the polymer backbone. This approach enabled the novel polymer to solidify oil using 10-undecenoic acid as cross-linking arms to produce a porous 3D polystyrene network with high mechanical strength. The powder poly(styrene-*co*-10-undecenoic) organogelator could gel oil from a biphasic mixture at a very low concentration of 5.5 mg /1 mL oil. The poly(styrene-*co*-

10-undecenoic) organogelator was also phase-selective due to the high hydrophobicity of polystyrene, increasing the oil solidification capacity.

The oil absorption tests showed that increasing the 10-undecenoic acid composition in the copolymer increased the gelation ability of the gelator due to its higher number of cross-linking points. On the other hand, higher 10-undecenoic acid contents decreased the copolymer solubility in the oil due to the polar carboxylic acid functional group. Therefore, depending on the oil type, an organogelator with specific 10-undecenoic acid composition would perform the best. Both formed gels in diluted bitumen and diesel showed high storage modulus, $10^4 - 10^6$ Pa, confirming that obtained organogels are stiff and strong. The organogelator can be applied as an oil solidifier in real field wavy environments. Further investigation of poly(styrene-*co*-10-undecenoic) organogels By FTIR revealed that the hydrogen bonding site in 10-undecenoic acid is the main moiety that promotes intermolecular interaction that form gels. Of course, styrene benzene rings and alkyl chains also enforce the gel structure via π - π stacking and van der Waals interactions.

Finally, I studied the effectiveness of the poly(styrene-*co*-10-undecenoic) by determining the amount of organogelator needed to solidify oil under different conditions. I investigated operational parameters (SOR and oil/solidifier contact time) and solidifier bulk density by removing diluted bitumen from the water surface. An SOR of 1:8, which is 2 times lower than the currently proposed in the literature, could efficiently solidify oil in 15 minutes. It should be taken into consideration that the cohesiveness and consistency of the obtained gels were excellent for industrial applications. I also studied the influence of the bulk density of the organogelator on the solidification efficiency using organogelators with different particle sizes. Higher powder bulk density (smaller particle sizes showing) led to better oil gelation efficiency, likely because of more uniform particle distribution on the oil surface and faster organogelator dissolution.

5.2 Recommendations

Polymers are mainly used as oil sorbents, but with limited application. However, polymeric solidifiers are a new class of oil spill responses that are environment-friendly and could solve some of issues associated with conventional techniques. Polymers can be designed with different functionalities to be used as solidifiers and, more specifically, as organogelators with broad applications. To date, there has not been a systematic study to develop a polymeric organogelator to remove oil in benchmark and real field studies.

The findings of this thesis gave rise to several areas that need further investigation:

- i. One area that has not been studied well is the effect of the physical and chemical properties of the polymer organogelator on oil gelation efficiency. A few limited studies discussed the preliminary application of polymers to oil spill gelation. However, polymer properties such as polymer hydrophobicity/ oleophilicity, polymer molecular weight, and copolymer compositions directly affect the organogelation of oil spills.
- ii. Another critical consideration to extend the application of polymer organogelators is their application in different conditions, such as the acidic and basic surrounding environment. The practical applications of polymer organogelators are in open fields under different chemical and physical conditions. Therefore, a polymeric solidifier with robust and tunable functionality is required to succeed in field applications.
- iii. As I tried in this thesis, applying bio-polymers in environmental remediation techniques is a new approach that will help develop sustainable and greener oil remediation methods. The functional comonomer 10-undecenoic acid, responsible for the excellent oil gelation results, is a derivative of castor oil. Fortunately, many studies are focusing on bio-

polymer modification for various applications. I believe more innovative and in-depth analyses of bio-polymers are needed to explore the potential application in oil/water treatment for industrial applications.

References

- [1] M. Fingas, *The Basics of Oil Spill Cleanup*, 3rd Edition. CRC Press, 2013. doi: 10.1201/B13686.
- [2] E. L. Schrader, “Remediation of floating, open water oil spills: Comparative efficacy of commercially available polypropylene sorbent booms,” *Environmental Geology and Water Sciences* 1991 17:2, vol. 17, no. 2, pp. 157–166, Mar. 1991, doi: 10.1007/BF01701571.
- [3] V. Broje and A. A. Keller, “Improved Mechanical Oil Spill Recovery Using an Optimized Geometry for the Skimmer Surface,” *Environ Sci Technol*, vol. 40, no. 24, pp. 7914–7918, Dec. 2006, doi: 10.1021/ES061842M.
- [4] A. M. Vibhute and K. M. Sureshan, “How Far Are We in Combating Marine Oil Spills by Using Phase-Selective Organogelators?,” *ChemSusChem*, vol. 13, no. 20, pp. 5343–5360, Oct. 2020, doi: 10.1002/CSSC.202001285.
- [5] H. Zhu, S. Qiu, W. Jiang, D. Wu, and C. Zhang, “Evaluation of electrospun polyvinyl chloride/polystyrene fibers as sorbent materials for oil spill cleanup,” *Environ Sci Technol*, vol. 45, no. 10, pp. 4527–4531, May 2011, doi: 10.1021/ES2002343.
- [6] A. Bazargan, J. Tan, and G. McKay, “Standardization of oil sorbent performance testing,” *J Test Eval*, vol. 43, no. 6, pp. 1271–1278, Nov. 2015, doi: 10.1520/JTE20140227.
- [7] D. Wu, L. Fang, Y. Qin, W. Wu, C. Mao, and H. Zhu, “Oil sorbents with high sorption capacity, oil/water selectivity and reusability for oil spill cleanup,” *Mar Pollut Bull*, vol. 84, no. 1–2, pp. 263–267, Jul. 2014, doi: 10.1016/J.MARPOLBUL.2014.05.005.

- [8] H. X. Jin, B. Dong, B. Wu, and M. H. Zhou, "Oil Absorptive Polymers: Where Is the Future?," *Polym Plast Technol Eng*, vol. 51, no. 2, pp. 154–159, Jan. 2012, doi: 10.1080/03602559.2011.618167.
- [9] L. Tan and B. Tan, "Hypercrosslinked porous polymer materials: Design, synthesis, and applications," *Chem Soc Rev*, vol. 46, no. 11, pp. 3322–3356, 2017, doi: 10.1039/c6cs00851h.
- [10] J. Ge, H. Y. Zhao, H. W. Zhu, J. Huang, L. A. Shi, and S. H. Yu, "Advanced Sorbents for Oil-Spill Cleanup: Recent Advances and Future Perspectives," *Advanced Materials*, vol. 28, no. 47, pp. 10459–10490, 2016, doi: 10.1002/adma.201601812.
- [11] T. Miyata, A. Jikihara, K. Nakamae, and A. S. Hoffman, "Preparation of poly(2-glucosyloxyethyl methacrylate)-concanavalin A complex hydrogel and its glucose-sensitivity," *Macromol Chem Phys*, vol. 197, no. 3, pp. 1135–1146, 1996, doi: 10.1002/MACP.1996.021970330.
- [12] P. Wang, *Smart Materials for Advanced Environmental Applications*. 2016. doi: 10.1039/9781782622130-FP007.
- [13] B. Singh, S. Kumar, B. Kishore, and T. N. Narayanan, "Magnetic scaffolds in oil spill applications," *Environ Sci (Camb)*, vol. 6, no. 3, pp. 436–463, Mar. 2020, doi: 10.1039/C9EW00697D.
- [14] M. M. S. Abdullah, H. A. Al-Lohedan, and A. M. Atta, "Novel magnetic iron oxide nanoparticles coated with sulfonated asphaltene as crude oil spill collectors," *RSC Adv*, vol. 6, no. 64, pp. 59242–59249, Jun. 2016, doi: 10.1039/C6RA09651D.
- [15] A. M. Atta, H. A. Al-Lohedan, and S. A. Al-Hussain, "Functionalization of Magnetite Nanoparticles as Oil Spill Collector," *International Journal of Molecular Sciences* 2015,

- Vol. 16, Pages 6911-6931*, vol. 16, no. 4, pp. 6911–6931, Mar. 2015, doi: 10.3390/IJMS16046911.
- [16] D. Dave and A. E. Ghaly, “Remediation Technologies for Marine Oil Spills: A Critical Review and Comparative Analysis,” *Am J Environ Sci*, vol. 7, no. 5, pp. 423–440, Nov. 2011, doi: 10.3844/AJESSP.2011.423.440.
- [17] S. Ko *et al.*, “RETRACTED ARTICLE: Amine functionalized magnetic nanoparticles for removal of oil droplets from produced water and accelerated magnetic separation,” *Journal of Nanoparticle Research 2017 19:4*, vol. 19, no. 4, pp. 1–14, Mar. 2017, doi: 10.1007/S11051-017-3826-6.
- [18] F. L. Motta, S. R. Stoyanov, and J. B. P. Soares, “Application of solidifiers for oil spill containment: A review,” *Chemosphere*, vol. 194, pp. 837–846, 2018, doi: 10.1016/j.chemosphere.2017.11.103.
- [19] F. Merv, “A Review of Literature Related to Oil Spill Solidifiers 1990-2008 | Prince William Sound.” https://www.pwsrca.org/wpfb-file/review_of_oss_literature-pdf-2/ (accessed Jun. 15, 2022).
- [20] A. Ghalambor, “The effectiveness of solidifiers for combating oil spills,” *Louisiana Applied Oil Spill Research and Development Program. OSRADP Technical Report Series 96-006*, 1997.
- [21] F. L. Motta, S. R. Stoyanov, and J. B. P. Soares, “Development and application of an amylopectin-graft-poly(methyl acrylate) solidifier for rapid and efficient containment and recovery of heavy oil spills in aqueous environments,” *Chemosphere*, vol. 236, Dec. 2019, doi: 10.1016/j.chemosphere.2019.124352.

- [22] M. Fingas, “Review of Solidifiers: An Update 2013. The opinions in this PWSRCAC-commissioned report are not necessarily those of PWSRCAC.,” 2013.
- [23] M. Suzuki and K. Hanabusa, “Polymer organogelators that make supramolecular organogels through physical cross-linking and self-assembly,” *Chem Soc Rev*, vol. 39, no. 2, pp. 455–463, Jan. 2010, doi: 10.1039/b910604a.
- [24] R. G. Weiss and P. Terech, *Molecular Gels*. Dordrecht: Springer Netherlands, 2006. doi: 10.1007/1-4020-3689-2.
- [25] L. Yan, G. Li, Z. Ye, F. Tian, and S. Zhang, “Dual-responsive two-component supramolecular gels for self-healing materials and oil spill recovery,” *Chemical Communications*, vol. 50, no. 94, pp. 14839–14842, Oct. 2014, doi: 10.1039/c4cc07509a.
- [26] B. Eftekhari-Sis, A. Bagheri, H. Younesi Araghi, A. Akbari, and M. F. Paige, “Supramolecular self-assembly of oleylamide into organogels and hydrogels: a simple approach in phase selective gelation of oil spills,” *Soft Mater*, vol. 18, no. 1, pp. 55–66, Jan. 2020, doi: 10.1080/1539445X.2019.1684948.
- [27] M. Nandi, B. Maiti, S. Banerjee, and P. De, “Hydrogen bonding driven self-assembly of side-chain amino acid and fatty acid appended poly(methacrylate)s: Gelation and application in oil spill recovery,” *J Polym Sci A Polym Chem*, vol. 57, no. 4, pp. 511–521, Feb. 2019, doi: 10.1002/POLA.29289.
- [28] C. Zhuan, Y. Li, X. Yuan, J. Zhao, and X. Hou, “A sorbitol-based phase-selective organogelator for crude oil spills treatment,” *J Appl Polym Sci*, vol. 136, no. 6, p. 47052, Feb. 2019, doi: 10.1002/APP.47052.
- [29] M. Suzuki, C. Setoguchi, H. Shirai, and K. Hanabusa, “Organogelation by polymer organogelators with a L-lysine derivative: Formation of a three-dimensional network

- consisting of supramolecular and conventional polymers,” *Chemistry - A European Journal*, vol. 13, no. 29, pp. 8193–8200, 2007, doi: 10.1002/chem.200700146.
- [30] Y. Ohsedo, “Low-molecular-weight organogelators as functional materials for oil spill remediation,” *Polym Adv Technol*, vol. 27, no. 6, pp. 704–711, Jun. 2016, doi: 10.1002/PAT.3712.
- [31] K. Hanabusa and M. Suzuki, “Development of low-molecular-weight gelators and polymer-based gelators,” *Polymer Journal*, vol. 46, no. 11. Nature Publishing Group, pp. 776–782, Nov. 13, 2014. doi: 10.1038/pj.2014.64.
- [32] J. Raeburn, A. Z. Cardoso, and D. J. Adams, “The importance of the self-assembly process to control mechanical properties of low molecular weight hydrogels,” *Chem. Soc. Rev*, vol. 42, p. 5143, 2013, doi: 10.1039/c3cs60030k.
- [33] S. Bhattacharya and Y. Krishnan-Ghosh, “First report of phase selective gelation of oil from oil/water mixtures. Possible implications toward containing oil spills,” *Chemical Communications*, no. 2, pp. 185–186, Jan. 2001, doi: 10.1039/B007848O.
- [34] C. Ren, F. Chen, F. Zhou, J. Shen, H. Su, and H. Zeng, “Low-Cost Phase-Selective Organogelators for Rapid Gelation of Crude Oils at Room Temperature,” *Langmuir*, vol. 32, no. 50, pp. 13510–13516, Dec. 2016, doi: 10.1021/acs.langmuir.6b04027.
- [35] A. Prathap and K. M. Sureshan, “Sugar-Based Organogelators for Various Applications,” *Langmuir*, vol. 35, no. 18, pp. 6005–6014, May 2019, doi: 10.1021/acs.langmuir.9b00506.
- [36] A. M. Vibhute, V. Muvvala, and K. M. Sureshan, “A Sugar-Based Gelator for Marine Oil-Spill Recovery,” *Angewandte Chemie - International Edition*, vol. 55, no. 27, pp. 7782–7785, Jun. 2016, doi: 10.1002/anie.201510308.

- [37] M. Nandi, S. Banerjee, and P. De, “Stearoyl-appended pendant amino acid-based hyperbranched polymers for selective gelation of oil from oil/water mixtures,” *Polym Chem*, vol. 10, no. 14, pp. 1795–1805, Apr. 2019, doi: 10.1039/c9py00105k.
- [38] H. Yao, L. P. Yang, Z. feng He, J. R. Li, and W. Jiang, “A phase-selective, bis-urea organogelator with a curved bis-naphthalene core,” *Chinese Chemical Letters*, vol. 28, no. 4, pp. 782–786, Apr. 2017, doi: 10.1016/J.CCLET.2016.12.031.
- [39] N. P. Pathak, Rajkamal, and S. Yadav, “A gelator–starch blend for dry powder based instant solidification of crude oil at room temperature,” *Chemical Communications*, vol. 56, no. 20, pp. 2999–3002, Mar. 2020, doi: 10.1039/C9CC09943C.
- [40] X. Zhang *et al.*, “Mandelic acid-derived organogelators: applications of their solid form in rapid and efficient remediation of marine oil spills,” *Mater Chem Front*, vol. 4, no. 1, pp. 222–230, Dec. 2019, doi: 10.1039/C9QM00603F.
- [41] M. Girolamo, A. Keller, K. Miyasaka, and N. Overbergh, “Gelation-crystallization in isotactic polystyrene solutions and its implications to crystal morphology, to the origin and structure of gels, and to the chemical homogeneity of polyolefins,” *Journal of Polymer Science: Polymer Physics Edition*, vol. 14, no. 1, pp. 39–61, Jan. 1976, doi: 10.1002/pol.1976.180140104.
- [42] M. Kobayashi, T. Nakaoki, and N. Ishihara, “Molecular conformation in glasses and gels of syndiotactic and isotactic polystyrenes,” *Macromolecules*, vol. 23, no. 1, pp. 78–83, Jan. 1990, doi: 10.1021/ma00203a015.
- [43] C. Daniel, D. Alfano, G. Guerra, and P. Musto, “Evaluation of the Amount and Composition of the Polymer-Rich and Polymer-Poor Phases of Syndiotactic Polystyrene Gels with

- Binary Solvent Mixtures,” *Macromolecules*, vol. 36, no. 15, pp. 5742–5750, Jul. 2003, doi: 10.1021/ma034430w.
- [44] H. Ihara *et al.*, “Novel self-assembling organogelators by combination of a double chain-alkylated L-glutamide and a polymeric head group,” *Org Biomol Chem*, vol. 1, no. 17, pp. 3004–3006, Aug. 2003, doi: 10.1039/B305928F.
- [45] M. Boufadel, B. Chen, J. Foght, P. Hodson, S. Swanson, and A. Venosa, “The Royal Society of Canada Expert Panel: The Behaviour and Environmental Impacts of Crude Oil Released into Aqueous Environments,” 2015, Accessed: Aug. 30, 2022. [Online]. Available: <http://www.rsc.ca/en/expert-panels/information-about-expert-panels>
- [46] D. Sundaravadivelu, M. T. Suidan, A. D. Venosa, P. I. Rosales, P. Campo-Moreno, and R. N. Conmy, “Development of a testing protocol for oil solidifier effectiveness evaluation,” *Clean Technol Environ Policy*, vol. 18, no. 4, pp. 1141–1150, Apr. 2016, doi: 10.1007/s10098-016-1107-1.
- [47] M. Fingas, *The Basics of Oil Spill Cleanup*, 3rd ed. Boca Raton, FL, USA: CRC Press, 2012. doi: 10.1201/b13686.
- [48] L. Yu, G. Hao, J. Gu, S. Zhou, N. Zhang, and W. Jiang, “Fe₃O₄/PS magnetic nanoparticles: Synthesis, characterization and their application as sorbents of oil from waste water,” *J Magn Magn Mater*, vol. 394, pp. 14–21, 2015, doi: 10.1016/j.jmmm.2015.06.045.
- [49] P. Henrique, C. Camargo, K. G. Satyanarayana, and F. Wypych, “Nanocomposites : Synthesis , Structure , Properties and New Application Opportunities,” *Materials Research*, vol. 12, no. 1, pp. 1–39, 2009, doi: 10.1590/S1516-14392009000100002.

- [50] P. Thanikaivelan, N. T. Narayanan, B. K. Pradhan, and P. M. Ajayan, “Collagen based magnetic nanocomposites for oil removal applications,” *Sci Rep*, vol. 2, 2012, doi: 10.1038/srep00230.
- [51] A. Turco, C. Malitesta, G. Barillaro, A. Greco, A. Maffezzoli, and E. Mazzotta, “A magnetic and highly reusable macroporous superhydrophobic/superoleophilic PDMS/MWNT nanocomposite for oil sorption from water,” *J Mater Chem A Mater*, vol. 3, no. 34, pp. 17685–17696, 2015, doi: 10.1039/c5ta04353k.
- [52] A. Pavia-Sanders, S. Zhang, J. A. Flores, J. E. Sanders, J. E. Raymond, and K. L. Wooley, “Robust magnetic/polymer hybrid nanoparticles designed for crude oil entrapment and recovery in aqueous environments,” *ACS Nano*, vol. 7, no. 9, pp. 7552–7561, 2013, doi: 10.1021/nn401541e.
- [53] Q. Zhu, F. Tao, and Q. Pan, “Fast and selective removal of oils from water surface via highly hydrophobic core-shell Fe₂O₃@C nanoparticles under magnetic field,” *ACS Applied Materials and Interfaces*, vol. 2, no. 11, pp. 3141–3146, 2010. doi: 10.1021/am1006194.
- [54] G. Simonsen, M. Strand, and G. Øye, “Potential applications of magnetic nanoparticles within separation in the petroleum industry,” *Journal of Petroleum Science and Engineering*, vol. 165, pp. 488–495, 2018. doi: 10.1016/j.petrol.2018.02.048.
- [55] J. A. Flores, A. Pavia-Sanders, Y. Chen, D. J. Pochan, and K. L. Wooley, “Recyclable hybrid inorganic/organic magnetically active networks for the sequestration of crude oil from aqueous environments,” *Chemistry of Materials*, vol. 27, no. 10, pp. 3775–3782, May 2015, doi: 10.1021/acs.chemmater.5b01523.

- [56] F. G. De Souza, J. A. Marins, C. H. M. Rodrigues, and J. C. Pinto, "A magnetic composite for cleaning of oil spills on water," *Macromolecular Materials and Engineering*, vol. 295, no. 10, pp. 942–948, 2010. doi: 10.1002/mame.201000090.
- [57] P. Li, B. Yu, and X. Wei, "Synthesis and characterization of a high oil-absorbing magnetic composite material," *Journal of Applied Polymer Science*, vol. 93, no. 2, pp. 894–900, 2004. doi: 10.1002/app.20522.
- [58] P. Calcagnile *et al.*, "Magnetically driven floating foams for the removal of oil contaminants from water," *ACS Nano*, vol. 6, no. 6, pp. 5413–5419, 2012, doi: 10.1021/nn3012948.
- [59] N. Chen and Q. Pan, "Versatile fabrication of ultralight magnetic foams and application for oil-water separation," *ACS Nano*, vol. 7, no. 8, pp. 6875–6883, Aug. 2013, doi: 10.1021/nn4020533.
- [60] A. Middea *et al.*, "Magnetic polystyrene–palygorskite nanocomposite obtained by heterogeneous phase polymerization to apply in the treatment of oily waters," *J Appl Polym Sci*, vol. 135, no. 15, p. 46162, Apr. 2018, doi: 10.1002/app.46162.
- [61] L. Yu, G. Hao, Q. Liang, S. Zhou, N. Zhang, and W. Jiang, "Facile preparation and characterization of modified magnetic silica nanocomposite particles for oil absorption," *Appl Surf Sci*, vol. 357, pp. 2297–2305, 2015, doi: 10.1016/j.apsusc.2015.09.231.
- [62] M. Chen *et al.*, "Synthesis of highly hydrophobic floating magnetic polymer nanocomposites for the removal of oils from water surface," *Appl Surf Sci*, vol. 286, pp. 249–256, 2013, doi: 10.1016/j.apsusc.2013.09.059.
- [63] N. A. Abdelwahab and M. A. Abd El-Ghaffar, "Preparation and characterization of highly hydrophobic magnetic polyaniline nanocomposite for fast and efficient separation of diesel

- oil from seawater,” *Mater Res Bull*, vol. 84, pp. 7–14, 2016, doi: 10.1016/j.materresbull.2016.07.022.
- [64] S. Patel and G. Hota, “Iron oxide nanoparticle-immobilized PAN nanofibers: synthesis and adsorption studies,” *RSC Adv*, vol. 6, no. 19, pp. 15402–15414, 2016, doi: 10.1039/C5RA20345G.
- [65] T. R. Fadel, J. A. Steevens, T. A. Thomas, and I. Linkov, “The challenges of nanotechnology risk management,” *Nano Today*, vol. 10, no. 1, pp. 6–10, 2015, doi: 10.1016/j.nantod.2014.09.008.
- [66] B. K. Sodipo and A. A. Aziz, “Recent advances in synthesis and surface modification of superparamagnetic iron oxide nanoparticles with silica,” *J Magn Magn Mater*, vol. 416, pp. 275–291, 2016, doi: 10.1016/j.jmmm.2016.05.019.
- [67] S. Natarajan, K. Harini, G. P. Gajula, B. Sarmiento, M. T. Neves-Petersen, and V. Thiagarajan, “Multifunctional magnetic iron oxide nanoparticles: diverse synthetic approaches, surface modifications, cytotoxicity towards biomedical and industrial applications,” *BMC Materials*, vol. 1, no. 1. 2019. doi: 10.1186/s42833-019-0002-6.
- [68] A. F. Avila, V. C. Munhoz, A. M. De Oliveira, M. C. G. Santos, G. R. B. S. Lacerda, and C. P. Gonçalves, “Nano-based systems for oil spills control and cleanup,” *J Hazard Mater*, vol. 272, pp. 20–27, 2014, doi: 10.1016/j.jhazmat.2014.02.038.
- [69] S. Mirshahghassemi and J. R. Lead, “Oil Recovery from Water under Environmentally Relevant Conditions Using Magnetic Nanoparticles,” *Environ Sci Technol*, vol. 49, no. 19, pp. 11729–11736, 2015, doi: 10.1021/acs.est.5b02687.

- [70] M. Sarcletti *et al.*, “Superoleophilic Magnetic Iron Oxide Nanoparticles for Effective Hydrocarbon Removal from Water,” *Advanced Functional Materials*, vol. 29, no. 15, 2019. doi: 10.1002/adfm.201805742.
- [71] K. Nagase *et al.*, “Thermoresponsive polymer brush surfaces with hydrophobic groups for all-aqueous chromatography,” *ACS Appl Mater Interfaces*, vol. 2, no. 4, pp. 1247–1253, 2010, doi: 10.1021/am100122h.
- [72] S. I. Uribe Madrid, U. Pal, and F. Sánchez-De Jesús, “Controlling size and magnetic properties of Fe₃O₄ clusters in solvothermal process,” *Adv Nano Res*, vol. 2, no. 4, pp. 187–198, 2014, doi: 10.12989/anr.2014.2.4.187.
- [73] I. J. Bruce and T. Sen, “Surface modification of magnetic nanoparticles with alkoxy silanes and their application in magnetic bioseparations,” *Langmuir*, vol. 21, no. 15, pp. 7029–7035, Jul. 2005, doi: 10.1021/LA050553T.
- [74] H. Yan, Z. Liping, H. Weiwei, L. Xiaojuan, L. Xiangnong, and Y. Yuxiang, “A study on synthesis and properties of Fe₃O₄ nanoparticles by solvothermal method,” *Glass Physics and Chemistry*, vol. 36, no. 3, pp. 325–331, 2010, doi: 10.1134/S1087659610030090.
- [75] Y. Tian, B. Yu, X. Li, and K. Li, “Facile solvothermal synthesis of monodisperse Fe₃O₄ nanocrystals with precise size control of one nanometre as potential MRI contrast agents,” *J Mater Chem*, vol. 21, no. 8, pp. 2476–2481, 2011, doi: 10.1039/c0jm02913k.
- [76] W. Cheng, K. Tang, Y. Qi, J. Sheng, and Z. Liu, “One-step synthesis of superparamagnetic monodisperse porous Fe₃O₄ hollow and core-shell spheres,” *J Mater Chem*, vol. 20, no. 9, pp. 1799–1805, Feb. 2010, doi: 10.1039/b919164j.

- [77] Y. Xie, R. Sougrat, and S. P. Nunes, "Synthesis and characterization of polystyrene coated iron oxide nanoparticles and asymmetric assemblies by phase inversion," *J Appl Polym Sci*, vol. 132, no. 5, p. 41368, Feb. 2015, doi: 10.1002/app.41368.
- [78] J. Fang, Y. Xuan, and Q. Li, "Preparation of polystyrene spheres in different particle sizes and assembly of the PS colloidal crystals," *Sci China Technol Sci*, vol. 53, no. 11, pp. 3088–3093, Nov. 2010, doi: 10.1007/s11431-010-4110-5.
- [79] K. Matyjaszewski and J. Xia, "Atom transfer radical polymerization," *Chem Rev*, vol. 101, no. 9, pp. 2921–2990, Sep. 2001, doi: 10.1021/cr940534g.
- [80] J. Xia and K. Matyjaszewski, "Controlled/'Living' Radical Polymerization. Homogeneous Reverse Atom Transfer Radical Polymerization Using AIBN as the Initiator," *Macromolecules*, vol. 30, no. 25, pp. 7692–7696, Dec. 1997, doi: 10.1021/ma9710085.
- [81] T. von Werne and T. E. Patten, "Atom transfer radical polymerization from nanoparticles: A tool for the preparation of well-defined hybrid nanostructures and for understanding the chemistry of controlled/'living" radical polymerizations from surfaces," *J Am Chem Soc*, vol. 123, no. 31, pp. 7497–7505, 2001, doi: 10.1021/ja010235q.
- [82] D. A. C. Thomson, E. H. L. Tee, N. T. D. Tran, M. J. Monteiro, and M. A. Cooper, "Oligonucleotide and polymer functionalized nanoparticles for amplification-free detection of DNA," *Biomacromolecules*, vol. 13, no. 6, pp. 1981–1989, Jun. 2012, doi: 10.1021/bm300717f.
- [83] J. Gu, W. Jiang, F. Wang, M. Chen, J. Mao, and T. Xie, "Facile removal of oils from water surfaces through highly hydrophobic and magnetic polymer nanocomposites," *Appl Surf Sci*, vol. 301, pp. 492–499, 2014, doi: 10.1016/j.apsusc.2014.02.112.

- [84] R. T. Carson, R. C. Mitchell, M. Hanemann, R. J. Kopp, S. Presser, and P. A. Ruud, “Contingent valuation and lost passive use: Damages from the Exxon Valdez oil spill,” *Environ Resour Econ (Dordr)*, vol. 25, no. 3, pp. 257–286, Jul. 2003, doi: 10.1023/A:1024486702104.
- [85] S. E. Allan, B. W. Smith, and K. A. Anderson, “Impact of the deepwater horizon oil spill on bioavailable polycyclic aromatic hydrocarbons in gulf of Mexico coastal waters,” *Environ Sci Technol*, vol. 46, no. 4, pp. 2033–2039, Feb. 2012, doi: 10.1021/ES202942Q.
- [86] M. Schrope, “Oil spill: Deep wounds,” *Nature*, vol. 472, no. 7342. Nature, pp. 152–154, Apr. 14, 2011. doi: 10.1038/472152a.
- [87] M. Cheng, Y. Gao, X. Guo, Z. Shi, J. F. Chen, and F. Shi, “A functionally integrated device for effective and facile oil spill cleanup,” *Langmuir*, vol. 27, no. 12, pp. 7371–7375, Jun. 2011, doi: 10.1021/la201168j.
- [88] M. Fingas, *Controlled in-situ burning of spilled oil | IOGP Publications library*, vol. IOGP Report 523. IPIECA-IOGP, 2016.
- [89] R. C. Prince, “Oil spill dispersants: Boon or bane?,” *Environ Sci Technol*, vol. 49, no. 11, pp. 6376–6384, Jun. 2015, doi: 10.1021/acs.est.5b00961.
- [90] H. X. Jin, B. Dong, B. Wu, and M. H. Zhou, “Oil Absorptive Polymers: Where Is the Future?,” *Polymer - Plastics Technology and Engineering*, vol. 51, no. 2, pp. 154–159, 2012, doi: 10.1080/03602559.2011.618167.
- [91] R. M. Atlas and T. C. Hazen, “Oil biodegradation and bioremediation: A tale of the two worst spills in U.S. history,” *Environ Sci Technol*, vol. 45, no. 16, pp. 6709–6715, Aug. 2011, doi: 10.1021/es2013227.
- [92] M. Fingas, *Oil Spill Science and Technology: Second Edition*, 2nd ed. 2016.

- [93] D. P. Prendergast and P. M. Gschwend, "Assessing the performance and cost of oil spill remediation technologies," *J Clean Prod*, vol. 78, pp. 233–242, Sep. 2014, doi: 10.1016/j.jclepro.2014.04.054.
- [94] J. Morris, J. Bietsch, K. Bashaw, and G. Wang, "Recently developed carbohydrate based gelators and their applications," *Gels*, vol. 7, no. 1. MDPI AG, pp. 1–61, 2021. doi: 10.3390/GELS7010024.
- [95] A. Prathap and K. M. Sureshan, "A mannitol based phase selective supergelator offers a simple, viable and greener method to combat marine oil spills," *Chemical Communications*, vol. 48, no. 43, pp. 5250–5252, May 2012, doi: 10.1039/C2CC31631E.
- [96] A. Prathap and K. M. Sureshan, "Organogelator-Cellulose Composite for Practical and Eco-Friendly Marine Oil-Spill Recovery," *Angew Chem Int Ed Engl*, vol. 56, no. 32, pp. 9405–9409, Aug. 2017, doi: 10.1002/ANIE.201704699.
- [97] G. Yu, X. Yan, C. Han, and F. Huang, "Characterization of supramolecular gels," *Chem Soc Rev*, vol. 42, no. 16, pp. 6697–6722, Jul. 2013, doi: 10.1039/c3cs60080g.
- [98] R. G. Weiss and P. T  rech, "Introduction," *Molecular Gels: Materials with Self-Assembled Fibrillar Networks*. Springer Netherlands, pp. 1–13, 2006. doi: 10.1007/1-4020-3689-2_1.
- [99] J. Chen *et al.*, "Amino Acid-Containing Phase-Selective Organogelators: A Water-Based Delivery System for Oil Spill Treatment," *ACS Omega*, vol. 5, no. 30, pp. 18758–18765, Aug. 2020, doi: 10.1021/acsomega.0c01821.
- [100] M. A. Rogers and R. G. Weiss, "Systematic modifications of alkane-based molecular gelators and the consequences to the structures and properties of their gels," *New Journal of Chemistry*, vol. 39, no. 2. Royal Society of Chemistry, pp. 785–799, 2015. doi: 10.1039/c4nj01439a.

- [101] H. Yu, B. Liu, Y. Wang, J. Wang, and Q. Hao, "Gallic ester-based phase-selective gelators," *Soft Matter*, vol. 7, no. 11, pp. 5113–5115, Jun. 2011, doi: 10.1039/c1sm05549f.
- [102] M. Yamanaka, "Urea derivatives as low-molecular-weight gelators," *Journal of Inclusion Phenomena and Macrocyclic Chemistry*, vol. 77, no. 1–4. Springer, pp. 33–48, Dec. 27, 2013. doi: 10.1007/s10847-013-0299-9.
- [103] S. R. Jadhav, P. K. Vemula, R. Kumar, S. R. Raghavan, and G. John, "Sugar-derived phase-selective molecular gelators as model solidifiers for oil spills," *Angewandte Chemie - International Edition*, vol. 49, no. 42, pp. 7695–7698, Oct. 2010, doi: 10.1002/anie.201002095.
- [104] S. Datta, S. Samanta, and D. Chaudhuri, "Near instantaneous gelation of crude oil using naphthalene diimide based powder gelator," *J Mater Chem A Mater*, vol. 6, no. 7, pp. 2922–2926, Feb. 2018, doi: 10.1039/c7ta10103a.
- [105] D. R. Trivedi and P. Dastidar, "Instant gelation of various organic fluids including petrol at room temperature by a new class of supramolecular gelators," *Chemistry of Materials*, vol. 18, no. 6, pp. 1470–1478, Mar. 2006, doi: 10.1021/cm0523586.
- [106] J. Li, Y. Huo, and H. Zeng, "Combinatorial identification of a highly soluble phase-selective organogelator with high gelling capacity for crude oil gelation," *J Mater Chem A Mater*, vol. 6, no. 22, pp. 10196–10200, Jun. 2018, doi: 10.1039/c8ta03415j.
- [107] D. Wang, J. Niu, Z. Wang, and J. Jin, "Monoglyceride-Based Organogelator for Broad-Range Oil Uptake with High Capacity," *Langmuir*, vol. 31, no. 5, pp. 1670–1674, Feb. 2015, doi: 10.1021/acs.langmuir.5b00053.

- [108] D. Dasgupta and J.-M. Guenet, “The Solvent in Physical Gelation: Polymers Versus Organogelators,” *Macromol Chem Phys*, vol. 214, no. 17, pp. 1885–1892, Sep. 2013, doi: <https://doi.org/10.1002/macp.201300094>.
- [109] A. Saiani, “Gelation dynamics and mechanism(s) in stereoregular poly(methyl methacrylate)s,” in *Macromolecular Symposia*, 2005, vol. 222, pp. 37–48. doi: 10.1002/masy.200550404.
- [110] C. Daniel, A. Avallone, and G. Guerra, “Syndiotactic polystyrene physical gels: Guest influence on structural order in molecular complex domains and gel transparency,” *Macromolecules*, vol. 39, no. 22, pp. 7578–7582, Oct. 2006, doi: 10.1021/ma061124k.
- [111] J. Chang, Q. Zhao, L. Kang, H. Li, M. Xie, and X. Liao, “Multiresponsive Supramolecular Gel Based on Pillararene-Containing Polymers,” *Macromolecules*, vol. 49, no. 7, pp. 2814–2820, Apr. 2016, doi: 10.1021/acs.macromol.6b00270.
- [112] X. Yu, X. Chen, Q. Chai, and N. Ayres, “Synthesis of polymer organogelators using hydrogen bonding as physical cross-links,” *Colloid Polym Sci*, vol. 294, no. 1, pp. 59–68, Jan. 2016, doi: 10.1007/s00396-015-3797-z.
- [113] D. Dasgupta, S. Srinivasan, C. Rochas, A. Ajayaghosh, and J. M. Guenet, “Hybrid thermoreversible gels from covalent polymers and organogels,” *Langmuir*, vol. 25, no. 15, pp. 8593–8598, Aug. 2009, doi: 10.1021/LA804185Q.
- [114] S. N. Khot *et al.*, “Development and application of triglyceride-based polymers and composites,” *J Appl Polym Sci*, vol. 82, no. 3, pp. 703–723, Oct. 2001, doi: 10.1002/app.1897.

- [115] K. Soundarajan and T. Mohan Das, “Sugar-benzohydrazide based phase selective gelators for marine oil spill recovery and removal of dye from polluted water,” *Carbohydr Res*, vol. 481, pp. 60–66, Jul. 2019, doi: 10.1016/j.carres.2019.06.011.
- [116] Z. Yang, G. Liang, and B. Xu, “Supramolecular hydrogels based on β -amino acid derivatives,” *Chemical Communications*, no. 7, pp. 738–740, 2006, doi: 10.1039/B516133A.
- [117] C.-C. Tsai *et al.*, “Biscalix[4]arene Derivative As a Very Efficient Phase Selective Gelator for Oil Spill Recovery,” *Org Lett*, vol. 15, no. 22, pp. 5830–5833, Nov. 2013, doi: 10.1021/ol402898u.
- [118] Y. Cui, M. C. Li, Q. Wu, J. A. Pojman, and D. G. Kuroda, “Synthesis-free phase-selective gelator for oil-spill remediation,” *ACS Appl Mater Interfaces*, vol. 9, no. 39, pp. 33549–33553, Oct. 2017, doi: 10.1021/acsami.7b10009.
- [119] M. Nandi, S. Pan, D. Ghosh, and P. De, “Effects of Main-chain and Chain-ends on the Organogelation of Stearoyl Appended Pendant Valine Based Polymers,” *Chinese J. Polym. Sci* 2019, vol. 37, no. 9, pp. 903–911, Sep. 2019, doi: 10.1007/S10118-019-2265-5.
- [120] V. Chandrasekaran, L. Biennier, E. Arunan, D. Talbi, and R. Georges, “Direct infrared absorption spectroscopy of benzene dimer,” *Journal of Physical Chemistry A*, vol. 115, no. 41, pp. 11263–11268, Oct. 2011, doi: 10.1021/JP204628G.
- [121] S. Ganguly *et al.*, “Understanding Structural Variations in Elastic Organic Crystals by in Situ High-Pressure Fourier Transform Infrared Spectroscopy and Nanoindentation Study,” *Cryst Growth Des*, vol. 19, no. 4, pp. 2114–2122, Apr. 2019, doi: 10.1021/acs.cgd.8b01684.

- [122] F. L. Motta, S. R. Stoyanov, and J. B. P. Soares, “Application of solidifiers for oil spill containment: A review,” *Chemosphere*, vol. 194. Elsevier Ltd, pp. 837–846, Mar. 01, 2018. doi: 10.1016/j.chemosphere.2017.11.103.
- [123] M. Fingas and B. Fieldhouse, “Review of Solidifiers,” in *Oil Spill Science and Technology*, Elsevier Inc., 2011, pp. 713–733. doi: 10.1016/B978-1-85617-943-0.10022-X.
- [124] R. D. Delaune, C. W. Lindau, and A. Jugsujinda, “Effectiveness of ‘Nochar’ Solidifier Polymer in Removing Oil from Open Water in Coastal Wetlands,” *Spill Science & Technology Bulletin*, vol. 5, no. 5–6, pp. 357–359, Oct. 1999, doi: 10.1016/S1353-2561(99)00081-X.
- [125] M. F. Fingas, R. Stoodley, and N. Laroche, “Effectiveness testing of spill-treating agents,” *Oil and Chemical Pollution*, vol. 7, no. 4, pp. 337–348, Jan. 1990, doi: 10.1016/S0269-8579(05)80048-6.
- [126] C. E. Brown, B. Fieldhouse, T. C. Lumley, P. Lambert, and B. P. Hollebhone, “Environment Canada’s Methods for Assessing Oil Spill Treating Agents,” in *Oil Spill Science and Technology*, Elsevier Inc., 2011, pp. 643–671. doi: 10.1016/B978-1-85617-943-0.10019-X.
- [127] M. F. Fingas’ and E. J. Tennyson, “Chemical treating agents for oil spill response—Recent research results,” in *Proceedings of the seventh Symposium on Coastal and Ocean Management, Long Beach, United States.*, 1991, pp. 8–12.
- [128] P. I. Rosales, M. T. Suidan, and A. D. Venosa, “A laboratory screening study on the use of solidifiers as a response tool to remove crude oil slicks on seawater,” *Chemosphere*, vol. 80, no. 4, pp. 389–395, 2010, doi: 10.1016/j.chemosphere.2010.04.036.

- [129] D. Sundaravadivelu, M. T. Suidan, A. D. Venosa, and P. I. Rosales, “Characterization of solidifiers used for oil spill remediation,” *Chemosphere*, vol. 144, pp. 1490–1497, Feb. 2016, doi: 10.1016/j.chemosphere.2015.10.030.
- [130] D. Sundaravadivelu, M. T. Suidan, and A. D. Venosa, “Parametric study to determine the effect of temperature on oil solidifier performance and the development of a new empirical correlation for predicting effectiveness,” *Mar Pollut Bull*, vol. 95, no. 1, pp. 297–304, Jun. 2015, doi: 10.1016/j.marpolbul.2015.03.027.
- [131] N. Shojaei, F. Aminsharei, and H. Abbastabar Ahangar, “Application of hydrophobic polymers as solidifiers for oil spill cleanup,” *International Journal of Environmental Science and Technology*, vol. 18, no. 6, pp. 1419–1424, Jun. 2021, doi: 10.1007/s13762-020-02882-y.

Appendix A: Supplementary Information for Chapter 2

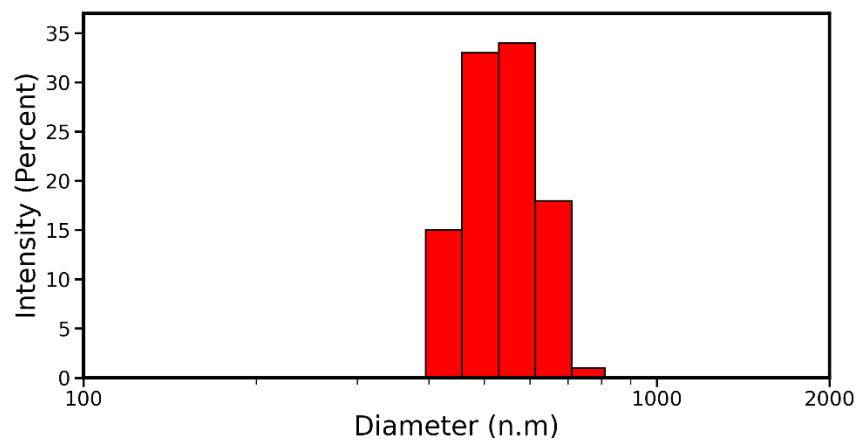


Figure A.1 Hydrodynamic size distribution of IONP determined by dynamic light scattering.

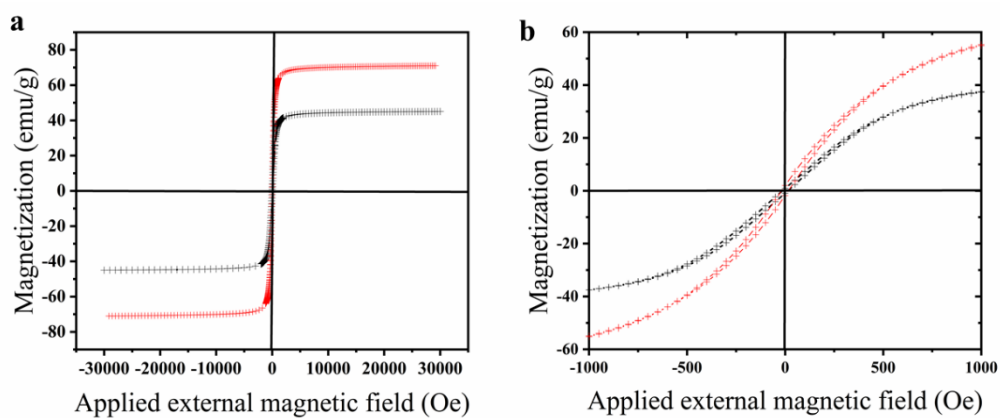


Figure A.2 Room temperature hysteresis of IONP (red) and SiO₂-IONP (black): a) full hysteresis loop, b) hysteresis in low field.

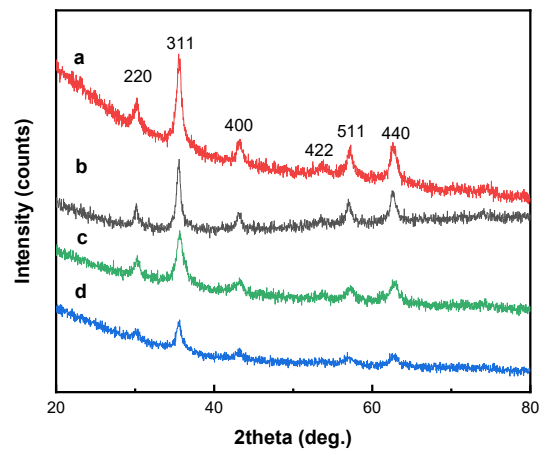


Figure A.3 XRD spectra: a) IONP, b) SiO₂-IONP, c) Br-SiO₂-IONP, and d) PS-SiO₂-IONP.

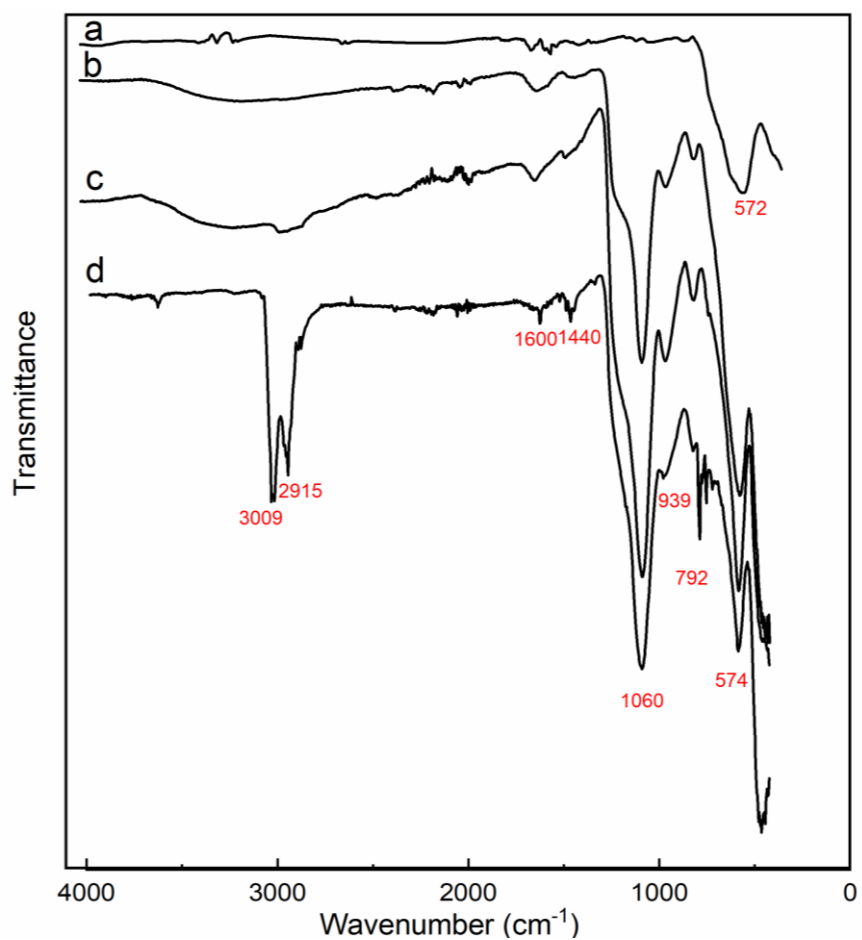


Figure A.4 FTIR spectra: a) IONP, b) SiO₂-IONP, c) Br-SiO₂-IONP, and d) PS-SiO₂-IONP.

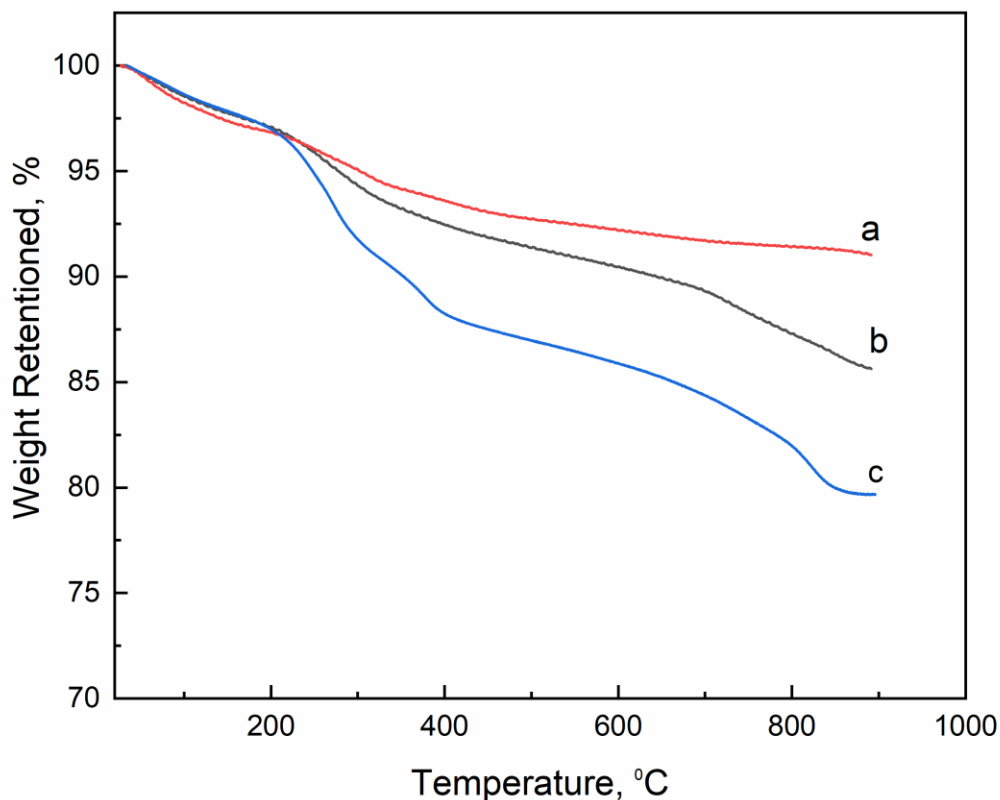


Figure A.5 TGA thermographs: a) SiO₂-IONP, b) Br-SiO₂-IONP, and c) PS-SiO₂-IONP.

Graft Density Calculation Using TGA Curves

The ATRP initiator graft density and polymer graft density were calculated by using equation (1).

$$\rho_g = \frac{\Delta w}{100 - \Delta w} \cdot \frac{\rho_p V_p N_A}{MS} \cdot 10^{-21} \quad (1)$$

where ρ_g is the grafting density in number of molecules per nm², Δw is the weight loss in each step in Figure S5, ρ_p is the density of the particles (2 g/cm³), V_p is the volume of the particles calculated from a radius of 395 nm, $N_A = 6.022 \times 10^{23}$ is Avogadro's number, M is the molar

mass of thermally decomposed moiety, and S is the surface area of the particles calculated from a radius of 395 nm.

ATRP Initiator Density Calculation

In Figure S5, the difference in mass loss between curve (a) and curve (b) at 400 °C was caused by full combustion of ATRP initiator (propyl bromine) coated on the surface of SiO₂-IONP. The weight loss difference is 0.96 ($\Delta w = 93.39 - 92.43$). Where $M = 121.9$ g/mol is the molar mass of combusted moiety (propyl bromine). The volume to the surface ratio of the spherical nanoparticles (V_p/S) is $\frac{r}{3}$. Where $r = 395$ nm is the radius of SiO₂-IONP. With substitution above numbers in equation (1), ATRP initiator graft density, equation (2), is calculated to be 12.60 molecules/nm².

$$\rho_g = \frac{0.96}{100 - 0.96} \cdot \frac{2 \times 395 \times 6.022 \times 10^{23}}{3 \times 121.9} \cdot 10^{-21} \quad (2)$$

Polymer graft density calculation:

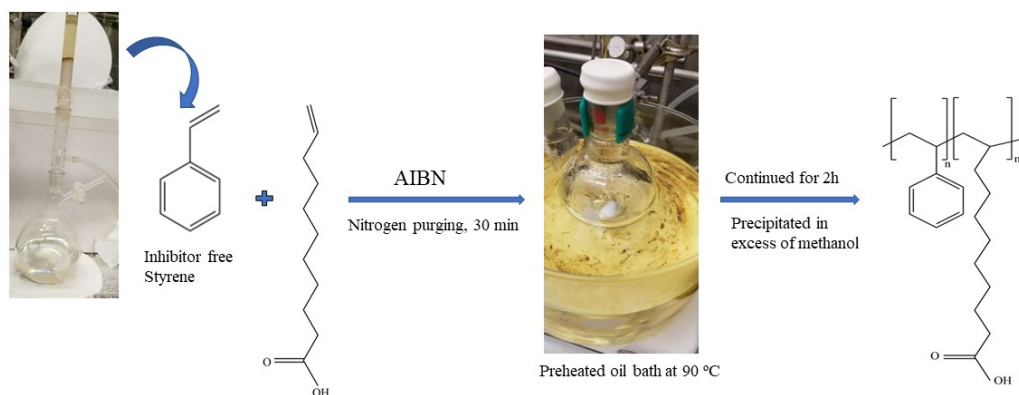
In Figure S5, the difference in mass loss between curve (b) and curve (c) at 400 °C was caused by full combustion of polystyrene grafted on the surface of SiO₂-IONP. The weight loss difference is 4.2 ($\Delta w = 92.43 - 88.23$). Where $M = 97,567$ g/mol is the GPC-measured M_n of the polymer. The volume to the surface ratio of the spherical nanoparticles (V_p/S) is $\frac{r}{3}$. Where $r = 395$ nm is the radius of SiO₂-IONP. Polymer graft density, equation (3), is calculated to be 0.0712 chains/nm².

$$\rho_g = \frac{4.2}{100 - 4.2} \cdot \frac{2 \times 395 \times 6.022 \times 10^{23}}{3 \times 97,567} \cdot 10^{-21} \quad (3)$$

Table A.1 PS/PS-SiO₂-IONP blends used in oil removal.

PS/PS-SiO ₂ -IONP blends	PS-SiO ₂ -IONP (20 mg) + PS (200 mg)
S1 blend	PS-SiO ₂ -IONP + PS ($M_n= 12,300$)
S2 blend	PS-SiO ₂ -IONP + PS ($M_n= 31,266$)
S3 blend	PS-SiO ₂ -IONP + PS ($M_n= 81,501$)
S4 blend	PS-SiO ₂ -IONP + PS ($M_n=97,567$)

Appendix B: Supplementary Information for Chapter 3



Scheme 1 Free radical polymerization of styrene and 10-undecenoic acid to make poly(styrene-*co*-10-undecenoic acid)

Calculation of poly(styrene-*co*-10-undecenoic acid) composition by $^1\text{H NMR}$

Poly(styrene-*co*-10-undecenoic acid) composition

We determined the copolymer composition ratio by comparing the characteristic resonance signals at 6.6-7.5 ppm from aromatic H (C_6H_5) in styrene against the aliphatic H ($-\text{CH}_2-$) shift at 2.3-2.37 ppm in 10-undecenoic acid. The copolymer composition was calculated from the area ratio under the curve for each comonomer's characteristic peaks. The area for each peak is normalized to the number of hydrogen atoms in the functional group. The sample spectra in Figure S2 represent the copolymer with 1.5 % 10-undecenoic acid. Equation (1) shows the 10-undecenoic acid comonomer composition calculation.

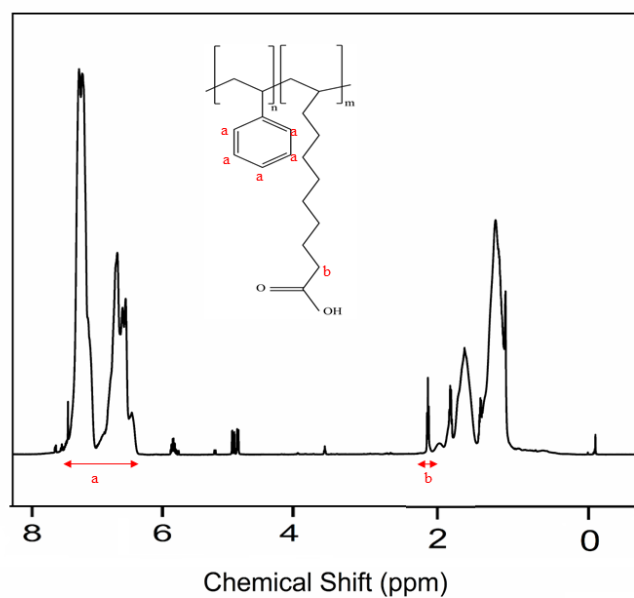


Figure B.1 HNMR sample spectra of poly(styrene-*co*-10-undecenoic acid)

$$F_{(10\text{-undecenoic acid})} = \frac{1/2 A_b}{1/5 A_a} \quad (1)$$

Where F is the comonomer composition of 10-undecenoic acid, A_a and A_b are the areas under the curve for peaks a and b, respectively.

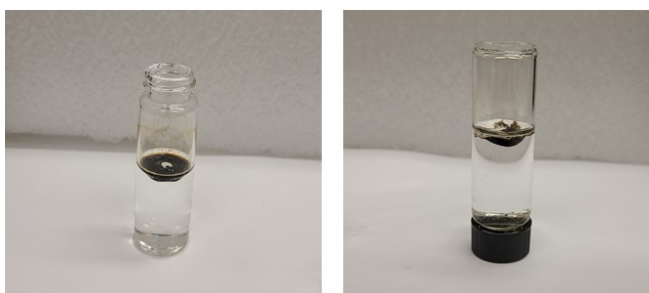


Figure B.2 Photographs of vial approach to measure the MGC.

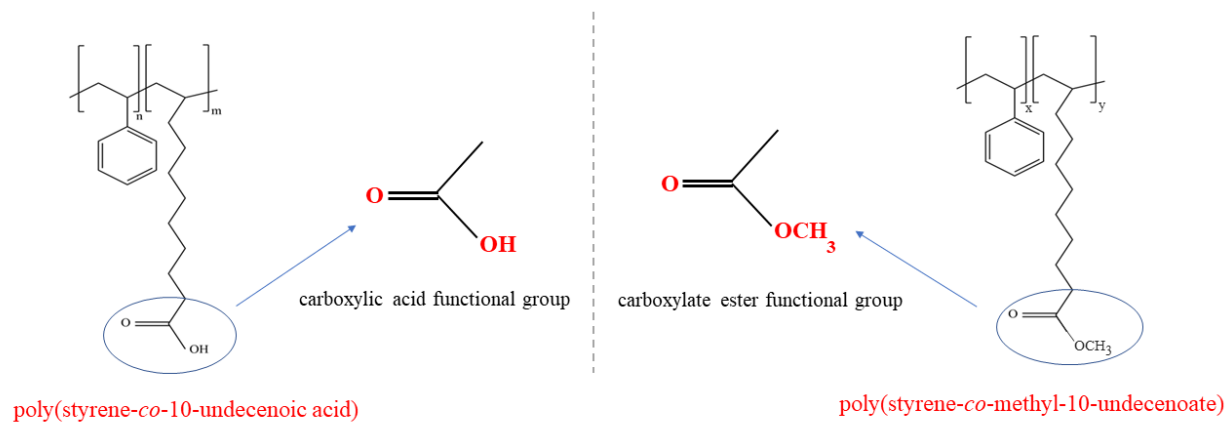


Figure B.3 Structures of poly(styrene-co-methyl-10-undecenoate) and poly(styrene-co-10-undecenoic acid).

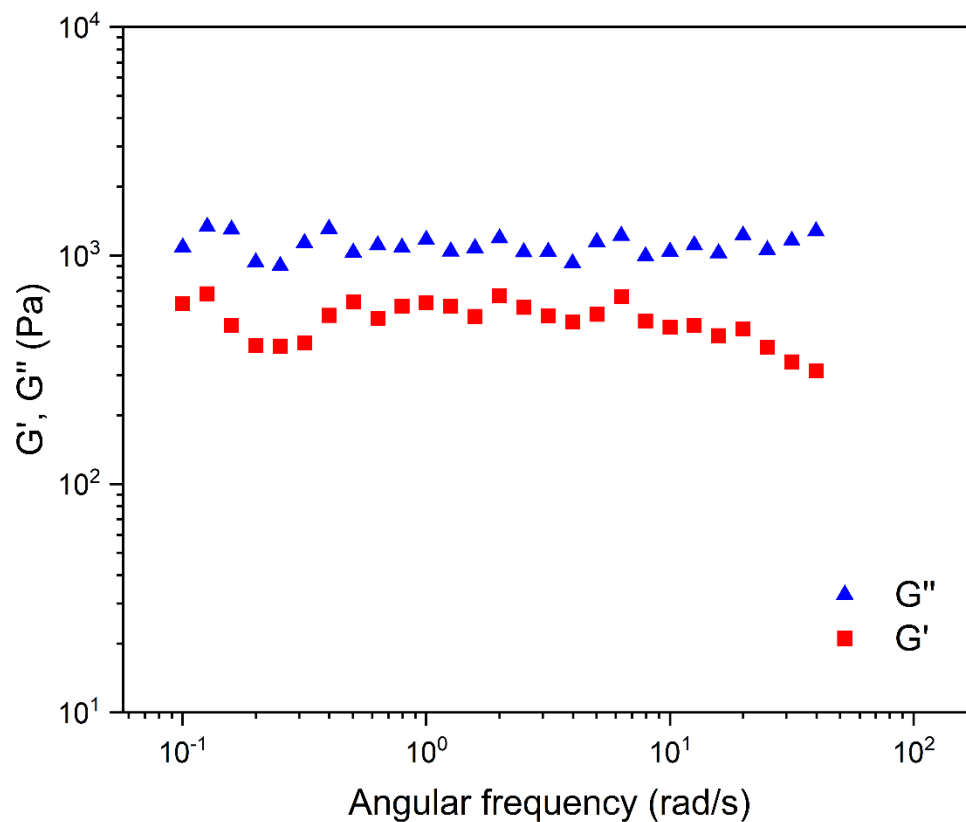


Figure B.4 Dynamic rheology studies of absorbed diesel by PSM10UA (15 mg polymer/100 μ L oil)

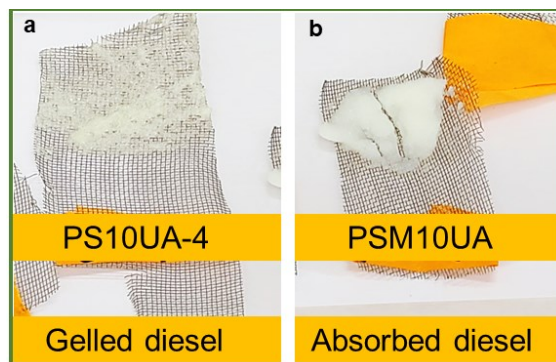


Figure B.5 Photograph of a) gelled diesel by PS10UA-4 (15 mg polymer/100 μ L oil), b) absorbed diesel by PSM10UA (15 mg polymer/100 μ L oil)

Appendix C: Supplementary Information for Chapter 4

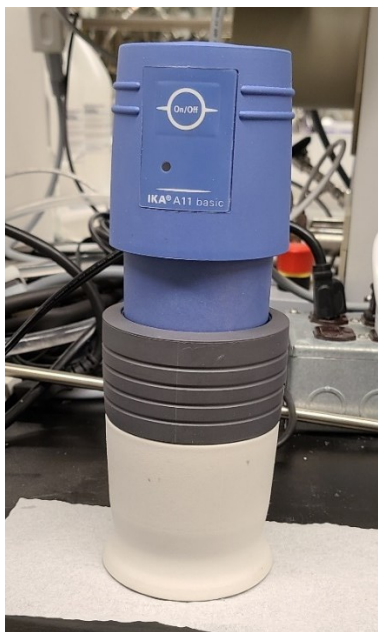


Figure C.1 Grinder used for milling POS



Figure C.2 Mechanical sieve shaker machine with different sieve mesh sizes (45, 250, 500, 850, 1000 μ).



Figure C.3 Final mat-like gelled-oil at the end of the oil removal experiments of diluted bitumen using POS. SOR of 1:8, 3 h.

Because some of the oil adhered to the walls of the petri dish, we repeated the 3 h test in a 1000 ml glass beaker.